On the modeling of fiber dispersion in fiber-reinforced elastic materials

Andrey V. Melnik*, Hudson Borja Da Rocha, Alain Goriely

OCCAM, Mathematical Institute, Oxford, UK

Abstract

When an isotropic material is subject to a uniaxial tension, the principal strain transverse to the direction of applied load is always negative. However, in fiber reinforced materials the transverse principal strain can change its sign as the load increases, passing through the zero-points, known as *perversions*. We investigate how the number of perversions in a material reinforced by two symmetrically aligned families of distributed fibers depends both on the degree of fiber dispersion and the model used for fiber dispersion. Angular integration and three variants of the generalized structure tensor approach are considered and discussed. The study of perversions clearly demonstrates the qualitative difference between these approaches in the case of high dispersion of fibers. The results suggest that this difference is primarily due to the way compressive fibers are modeled.

Keywords: fiber reinforced biological tissue, anisotropy, fiber dispersion, generalized structure tensor, uniaxial tension.

1 Introduction

In many soft biological tissues mechanical strength and anisotropy are determined primarily by the presence of fibers [8, 40], in particular collagen, which is the most abundant protein in mammals. Tissues differ in the amount, type, and spatial arrangement of collagen fibers, which are directly linked to the physiological functions tissues carry out and the mechanical loads they support [8]. For instance, collagen fibers in tendons are parallel and aligned in the direction of loading, while in the arterial wall a significant fiber dispersion around two preferred fiber directions is observed. As the internal structure of a tissue determines its mechanical properties, it is reasonable to include it in a constitutive model. The theory of nonlinear fiber-reinforced elastic composites [34, 35] asserts that the strain energy is in general expressed through a set of deformation invariants

*Corresponding author. Tel.: +44 1865 615146. E-mail address: andrey.melnik@maths.ox.ac.uk.
Postal address: Mathematical Institute, Radcliffe Observatory Quarter, Woodstock Road, Oxford OX2 6GG, UK.

and pseudo-invariants, whose number depends on the symmetry exhibited by the material. In this theory, fibers are thought as local special directions of anisotropy rather than as actual collagen fibrils. A popular *a priori* assumption in constitutive models is that the total stress generated by the whole tissue is the sum of stresses generated by its constituents [22, 23] (see also [20] and references therein). This assumption allows to incorporate quantitative data characterizing tissue's structure directly into the constitutive relation, *e.g.* fiber volume fraction or orientation-dependent density can be included as multiplicative factors in the appropriate term. In addition, structural approach allows to formulate phenomenological laws for fiber remodeling and study dynamics of mechanically induced fiber reorientation [5, 16, 25, 26].

In many studies it is assumed that fibers are oriented in a finite number of discrete directions (see *e.g.* [19, 15]). Continuous distribution of fiber directions was addressed by Lanir [22], who proposed a structural model for a planar collagenous tissue, where the total stress generated by fibers is given as an integral over the range of fiber directions. This approach, called the *angular integration* approach (AI), generalizes the cases of strict fiber alignment in several discrete directions, fiber dispersion around mean fiber directions and isotropic fiber distribution. The main disadvantage of this approach is that in most cases it requires repeated numerical integrations. Gasser et al. [10] proposed a material model which overcomes this drawback by using generalized structure tensors (GST). A similar approach was suggested by Freed et al. [9]. Models based on the GST approach were applied to many soft tissues, including human aortic valve [9], arterial wall [10, 20], cornea [29, 14], articulate cartilage [6] and bat wing membrane [38]. It has been noted that the GST and the AI approaches provide different predictions and that the error of the GST comparing to the AI model is small only for low fiber dispersion [3]. Recently a new model was suggested by Pandolfi and Vasta [30], in which they assumed that the fiber strain energy depends on the mean value and on the variance of fiber stretch. Their "V-model" is similar to the GST model in that it is justified by the Taylor expansion of the total fiber strain energy formulated according to the AI approach, but includes an additional term in the series. This idea was further developed by Cortes and Elliott, who introduced so-called generalized high-order structure tensors [2].

Motivated by the importance of accurate and numerically efficient constitutive models for elastic materials with distributed fiber reinforcement, we analyze the relation between the AI approach and several variants of the GST model (Figure 1), and compare the prediction they provide. In contrast other authors [3, 30], who use the relative error in stress as a measure of discrepancy between the models, we look for a qualitative attribute, and we chose as such the ability of an incompressible material to expand in the transverse direction when stretched. This feature is somewhat similar to having a direction-dependent Poisson's ratio, which is positive in one direction and negative in another direction. However, when a nonlinear material is being progressively stretched, the transverse extension can be followed by contraction and vice versa (Figure 6). These changes between contraction and extension are called the *perversion points* of the transverse strain [12]. The number of

these perversion points depends on the choice of model for dispersed fiber reinforcement and, therefore can be used to compare different models.

The paper is organized as follows. In Section 2 we give an overview of existing constitutive models for materials with distributed fibers, including angular integration (AI) and generalized structure tensor (GST) approaches. We discuss how to handle the issue of compressed fibers, making a clear distinction between the basic GST model and its variant for transversely isotropic distributions which is modified to exclude compressed fibers ("GSTx"). In Section 3 we formulate an alternative approach, based on partial angular integration. In Section 4 we formulate sufficient conditions imposed on orientation density functions for a material to be orthotropic and provide an example of multiply reinforced orthotropic material. In Section 5 we compare the various modeling approaches by applying them to the uniaxial tension of a material with two families of dispersed fibers.

2 Review of existing models

We use the framework of nonlinear elasticity and assume the existence of reference and deformed configurations ($\mathcal{B}_0$ and $\mathcal{B}$ respectively). Material points in $\mathcal{B}_0$ and $\mathcal{B}$ are related by a deformation $\boldsymbol{\chi}$, so that $\mathbf{x} = \boldsymbol{\chi}(\mathbf{X}) \in \mathcal{B}$, $\mathbf{X} \in \mathcal{B}_0$. We consider homogeneous hyperlastic incompressible materials, in which the strain energy (density) function $W(\mathbf{F})$ defines the dependence of the Cauchy stress $\boldsymbol{\sigma}$ on the deformation gradient $\mathbf{F} = \mathrm{grad}\boldsymbol{\chi} = [\partial x_i/\partial X_j]$. The stress-strain relation is

$$\boldsymbol{\sigma} = -p\mathbf{1} + \frac{\partial W}{\partial \mathbf{F}}\mathbf{F}^T, \tag{1}$$

where p is the Lagrangian multiplier related to the incompressibility condition $\det\mathbf{F} = 1$. The Cauchy equation of motion in mechanical equilibrium and in the absence of body forces reads

$$\mathrm{div}\boldsymbol{\sigma} = 0. \tag{2}$$

When restricted to the case of homogeneous deformations ($\mathbf{F} = \mathrm{const}$), equation (2) is automatically satisfied. The remaining stress-strain relation and the incompressibility condition allow then to compute the stress generated by a given deformation or the deformation if the stress is known from boundary conditions.

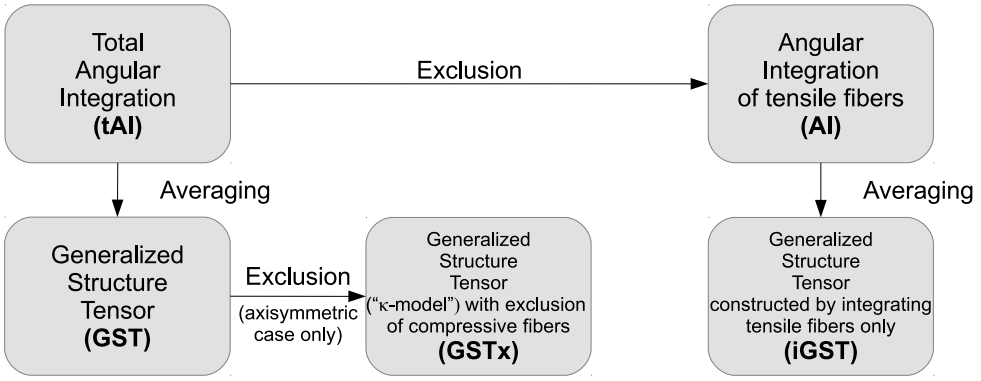

Figure 1: Relation between different modeling approaches for dispersed fiber reinforcement.

Name	Meaning	Definition
tAI	Total Angular Integration (not used in practice: AI is used instead)	$\Psi_{\mathrm{f}} = \oint\limits_{\mathbb{U}^2} \rho(\mathbf{m}_0)\psi_{\mathrm{f}}(\mathbf{m}_0 \otimes \mathbf{m}_0 : \mathbf{C})d\omega.$
AI	Angular Integration with fiber exclusion	$\Psi_{\mathrm{f}} = \oint\limits_{\mathbb{U}^2} \rho(\mathbf{m}_0)\chi(\mathbf{m}_0 \otimes \mathbf{m}_0 : \mathbf{C})\psi_{\mathrm{f}}(\mathbf{m}_0 \otimes \mathbf{m}_0 : \mathbf{C})d\omega.$
GST	Generalized Structure Tensor	$\Psi_{\mathrm{f}} = \mathrm{tr}\mathbf{H}\,\psi_{\mathrm{f}}(\frac{\mathbf{H}}{\mathrm{tr}\mathbf{H}} : \mathbf{C}), \quad \mathbf{H} = \oint\limits_{\mathbb{U}^2} \rho(\mathbf{m}_0)\mathbf{m}_0 \otimes \mathbf{m}_0 d\omega.$
GSTx	Generalized Structure Tensor with fiber exclusion	$\Psi_{\mathrm{f}} = \mathrm{tr}\mathbf{H}\,\psi_{\mathrm{f}}(\frac{\mathbf{H}}{\mathrm{tr}\mathbf{H}} : \mathbf{C}),$ $\mathbf{H} = \begin{cases} \kappa\mathbf{1} + (1-3\kappa)\mathbf{a}_0 \otimes \mathbf{a}_0, & (1-3\kappa)\,(\mathbf{a}_0 \otimes \mathbf{a}_0 : \mathbf{C} - 1) > 0, \\ \kappa\mathbf{1}, & \kappa \le \frac{1}{3}, \quad \mathbf{a}_0 \otimes \mathbf{a}_0 : \mathbf{C} \le 1, \\ (1-2\kappa)\mathbf{1}, & \kappa > \frac{1}{3}, \quad \mathbf{a}_0 \otimes \mathbf{a}_0 : \mathbf{C} \ge 1. \end{cases}$ $\kappa = \pi \int_0^{\pi} \tilde{\rho}(\theta)\sin^3\theta d\theta, \quad \text{where } \rho(\mathbf{m}_0) = \tilde{\rho}(\arccos \mathbf{m}_0.\mathbf{a}_0).$
iGST	Generalized Structure Tensor with selective fiber exclusion from the integrand	$\Psi_{\mathrm{f}} = \mathrm{tr}\mathbf{H}\,\psi_{\mathrm{f}}(\frac{\mathbf{H}}{\mathrm{tr}\mathbf{H}} : \mathbf{C}), \quad \mathbf{H} = \oint\limits_{\mathbb{U}^2} \rho(\mathbf{m}_0)\chi(\mathbf{m}_0 \otimes \mathbf{m}_0 : \mathbf{C})\,\mathbf{m}_0 \otimes \mathbf{m}_0 d\omega$

Table 1: Summary of models for dispersed fiber reinforcing.

Model	AI, tAI	GST, GSTx, iGST
Sufficient condition	$\sum_{i=1}^{m} \rho^{(i)}(\mathbf{m}_0) = \sum_{i=1}^{m} \rho^{(i)}(\mathbf{Q}\mathbf{m}_0),$ $\forall \mathbf{m}_0 \in \mathbb{U}^2, \forall \mathbf{Q} \in \mathbb{Q}.$	$\bigcup_i \rho^{(i)}(\mathbf{m}_0) = \bigcup_i \rho^{(i)}(\mathbf{Q}\mathbf{m}_0),$ $\forall \mathbf{m}_0 \in \mathbb{U}^2, \forall \mathbf{Q} \in \mathbb{Q}.$

Table 2: Conditions sufficient for symmetry of a material reinforced by mechanically equivalent fibers.

2.1 Angular integration (AI) approach for distributed fiber reinforcing

A strain energy function for an *isotropic hyperelastic material* can be expressed in terms of three scalar functions of a deformation tensor, which are known as the deformation invariants I_i. For an isotropic material one can write $W(\mathbf{F}) = \tilde{W}(\mathbf{C}) = \bar{W}(I_1, I_2, I_3)$, where $I_1 = \mathrm{tr}\mathbf{C}$, $I_2 = \frac{1}{2}(\mathrm{tr}^2\mathbf{C} - \mathrm{tr}\mathbf{C}^2)$, $I_3 = \det\mathbf{C}$, and $\mathbf{C} = \mathbf{F}^T\mathbf{F}$ is the right Cauchy-Green deformation tensor. A material reinforced by fibers perfectly aligned in one direction is an example of a *transversely isotropic material*, *i.e.* a material, which has one distinguished direction. A strain energy function for such material in general depends on a deformation tensor through five scalars, which consist of three isotropic deformation invariants I_1, I_2, I_3 and two extra (pseudo-)invariants, which are related to the strains in the fibers when deformed. Reinforcing by an additional family of fibers further reduces the symmetry of the material but extends the set of invariants from five to eight. These three extra scalars account for the strains in the second family and interactions between the two fiber families [34, 35, 18]. If the symmetry group of a material contains only the identity map $\mathbf{1}$ (and also $-\mathbf{1}$), then no conclusion regarding the form of the strain energy function can be made from symmetry considerations. This is the case of a general anisotropic material and the general case of a material reinforced by three or more fibers.

However, if the material is described as being multiply reinforced, then some information about the structure and composition must be available and can be used in the constitutive relation under certain assumptions. The assumptions, which allow to use this structural data can be: *(i)* the additive split of the strain energy function W into the isotropic part ψ_{iso} and the contributions of each fiber family $\psi_{\mathrm{f}}^{(i)}$; *(ii)* the dependence of fibers' contribution only on one scalar, *i.e.* $\psi_{\mathrm{f}}^{(i)} = \psi_{\mathrm{f}}^{(i)}(I_{\mathrm{f}}^{(i)})$. These assumptions have been used in several studies (see [20] and references therein), in which the strain energy function of a material has the form

$$W = \tilde{\psi}_{\mathrm{iso}}(\mathbf{C}) + \sum_i \rho^{(i)} \psi_{\mathrm{f}}^{(i)}(I_{\mathrm{f}}^{(i)}), \tag{3}$$

where $\rho^{(i)}$ is a weighting factor reflecting the amount of fibers in ith family, $I_{\mathrm{f}}^{(i)} = \mathbf{F}\mathbf{a}_0^{(i)}.\mathbf{F}\mathbf{a}_0^{(i)} = \mathbf{a}_0^{(i)} \otimes \mathbf{a}_0^{(i)} : \mathbf{C}$ is the square of fiber stretch, $\mathbf{a}_0^{(i)}$ is a unit vector in the ith family's direction and $(\tilde{\bullet})$ signifies that the quantity $(\bullet)$ is expressed as a function of $\mathbf{C}$ rather than a function of $\mathbf{F}$, which is always possible for isotropic functions.

If all fiber families are mechanically equivalent, *i.e.* $\psi_{\mathrm{f}}^{(i)}(I_{\mathrm{f}}^{(i)}) = \psi_{\mathrm{f}}(I_{\mathrm{f}}^{(i)})$, then (3) can be naturally generalized to the case of continuously distributed fibers

$$W = \tilde{\psi}_{\mathrm{iso}}(\mathbf{C}) + \oint_{\mathbb{U}^2} \rho\psi_{\mathrm{f}}(I_{\mathrm{f}})d\omega, \tag{4}$$

where $\mathbb{U}^2 = \{\mathbf{m}_0 \in \mathbb{R}^3, \text{ s.t. } |\mathbf{m}_0| = 1\}$ is the unit sphere, $d\omega$ is surface element area in the reference direction direction, $I_{\mathrm{f}} = \mathbf{m}_0 \otimes \mathbf{m}_0 : \mathbf{C}$ is the squared stretch in that direction, and $\rho = \rho(\mathbf{m}_0)$ is an *orientation density*

function (ODF), also called a *probability density function* by other authors. When a normalization condition is imposed, we use the form

$$\oint_{\mathbb{U}^2} \rho d\omega = 1. \tag{5}$$

as opposed to $\oint_{\mathbb{U}^2} \rho d\omega = 4\pi$, which is used in [10, 20, 30] (with the change $\rho \to \frac{1}{4\pi}\rho$ for comparison). Without loss of generality, it can be assumed that $\rho(\mathbf{m}_0) = \rho(-\mathbf{m}_0)$ holds, since the replacement $\rho(\mathbf{m}_0) \to \frac{1}{2}\left(\rho(\mathbf{m}_0) + \rho(-\mathbf{m}_0)\right)$ does not change the strain energy (4).

By analogy, the strain energy function of a material reinforced by m families of distributed fibers reads

$$W = \psi_{\text{iso}} + \Psi_{\text{f}}, \tag{6}$$

with

$$\Psi_{\text{f}} = \sum_{i=1}^{m} \oint_{\mathbb{U}^2} \rho^{(i)}(\mathbf{m}_0)\psi_{\text{f}}^{(i)}(I_{\text{f}})d\omega, \tag{7}$$

where the ith fiber family is characterized by a strain energy function $\psi_{\text{f}}^{(i)}$ and an ODF $\rho^{(i)}$. The Cauchy stress is then given by

$$\boldsymbol{\sigma} = -p\mathbf{1} + \boldsymbol{\sigma}_{\text{iso}} + \boldsymbol{\sigma}_{\text{f}} = -p\mathbf{1} + 2\mathbf{F}\frac{\partial \psi_{\text{iso}}}{\partial \mathbf{C}}\mathbf{F}^T + 2\mathbf{F}\frac{\partial \Psi_{\text{f}}}{\partial \mathbf{C}}\mathbf{F}^T. \tag{8}$$

When applying equation (8) directly to the strain energy (7) one obtains

$$\boldsymbol{\sigma}_{\text{f}} = 2\mathbf{F}\left(\sum_{i=1}^{m} \oint_{\mathbb{U}^2} \rho^{(i)}(\mathbf{m}_0)\psi_{\text{f}}^{(i)\prime}(I_{\text{f}})\mathbf{m}_0 \otimes \mathbf{m}_0 d\omega\right)\mathbf{F}^T. \tag{9}$$

This way of computing the Cauchy stress generated by fibers is called *angular integration* (AI) [3, 30, 33], as the total stress is given by angular integration of fiber fractions' stresses.

2.2 Exclusion of contracted fibers

In order to make sure that the fraction of undulated fibers does not contribute to the strain energy, one can introduce an additional multiplier χ into the integrand in (7), which takes values of 0 or 1 indicating whether fibers are compressed or not,

$$\chi(I_{\text{f}}) = \begin{cases} 1, & I_{\text{f}} = \mathbf{m}_0 \otimes \mathbf{m}_0 : \mathbf{C} > 1, \\ 0, & I_{\text{f}} = \mathbf{m}_0 \otimes \mathbf{m}_0 : \mathbf{C} \leq 1. \end{cases} \tag{10}$$

The total fiber strain energy and the Cauchy stress become

$$\Psi_{\mathrm{f}} = \sum_{i=1}^{m} \oint_{\mathbb{U}^2} \rho^{(i)}(\mathbf{m}_0)\chi(I_{\mathrm{f}})\psi_{\mathrm{f}}^{(i)}(I_{\mathrm{f}})d\omega, \tag{11}$$

$$\boldsymbol{\sigma}_{\mathrm{f}} = 2\mathbf{F}\left(\sum_{i=1}^{m} \oint_{\mathbb{U}^2} \rho^{(i)}(\mathbf{m}_0)\chi(I_{\mathrm{f}})\psi_{\mathrm{f}}^{(i)\prime}(I_{\mathrm{f}})\mathbf{m}_0 \otimes \mathbf{m}_0 d\omega\right)\mathbf{F}^T. \tag{12}$$

The conversion of (7) and (9) into (11) and (12) is equivalent to the modification of the fiber potential

$$\psi_{\mathrm{f}}^{(i)}(I_{\mathrm{f}}) \to \chi(I_{\mathrm{f}})\psi_{\mathrm{f}}^{(i)}(I_{\mathrm{f}}), \qquad \psi_{\mathrm{f}}^{(i)\prime}(I_{\mathrm{f}}) \to \chi(I_{\mathrm{f}})\psi_{\mathrm{f}}^{(i)\prime}(I_{\mathrm{f}}), \tag{13}$$

which is done to exclude the response of compressed fibers. An equivalent way of thinking about this conversion is to regard χ as the characteristic function of the set of tensile directions. This would correspond to a substitution

$$\rho^{(i)}(\mathbf{m}_0) \to \chi(I_{\mathrm{f}})\rho^{(i)}(\mathbf{m}_0), \tag{14}$$

wherein the implicit dependence of the left-hand side on the deformation tensor $\mathbf{C}$ is assumed.

Note that in the literature the factor χ may not be explicitly included in the equations (11), (12), yet the response of compressed fibers is excluded (*e.g.* as in [3]). Following [3, 30] we refer to the model (11), (12) with fiber exclusion as "AI". In order to further avoid ambiguity, we identify the model (7), (9), which integrates contracted fibers alongside with their extended counterparts, with the acronym "tAI" standing for the *total angular integration*.

2.3 Generalized structure tensor approach for distributed fiber reinforcing

The generalized structure tensor (GST) approach was introduced in [10] and is based on the truncated series expansion of the anisotropic part of strain energy in the tAI approach, as noticed in [30]. We provide the derivation of the GST model from the tAI approach, similar to the derivation given in [30], but without requiring the ODFs to be normalized. This difference is key for the correct formulation of the alternative GST model, as discussed in Section 3.

We define an averaging operator induced by an ODF ρ as

$$\langle \bullet \rangle_{\rho} = \oint_{\mathbb{U}^2} \rho(\mathbf{m}_0) \bullet d\omega, \tag{15}$$

where $\bullet$ denotes a scalar or tensor quantity. The normalized counterpart of (15) is defined by

$$[\bullet]_\rho = \frac{\langle \bullet \rangle_\rho}{\langle 1 \rangle_\rho} = \frac{\oint\limits_{\mathbb{U}^2} \rho(\mathbf{m}_0) \bullet d\omega}{\oint\limits_{\mathbb{U}^2} \rho(\mathbf{m}_0) d\omega}. \tag{16}$$

Consider the Taylor expansion of $\psi_{\mathrm{f}}(I_{\mathrm{f}})$ about $I_{\mathrm{f}} = [I_{\mathrm{f}}]_\rho$

$$\psi_{\mathrm{f}}(I_{\mathrm{f}}) = \psi_{\mathrm{f}}([I_{\mathrm{f}}]_\rho) + \psi_{\mathrm{f}}'([I_{\mathrm{f}}]_\rho) \cdot (I_{\mathrm{f}} - [I_{\mathrm{f}}]_\rho) + O\left((I_{\mathrm{f}} - [I_{\mathrm{f}}])_\rho)^2\right). \tag{17}$$

By omitting higher order terms and by applying $[\bullet]_\rho$ to both sides we obtain

$$[\psi_{\mathrm{f}}(I_{\mathrm{f}})]_\rho \approx \psi_{\mathrm{f}}([I_{\mathrm{f}}]_\rho)[1]_\rho + \psi_{\mathrm{f}}'([I_{\mathrm{f}}]_\rho) \cdot [(I_{\mathrm{f}} - [I_{\mathrm{f}}]_\rho)]_\rho. \tag{18}$$

Using $[1]_\rho = 1$ and $[I_{\mathrm{f}} - [I_{\mathrm{f}}]_\rho]_\rho = 0$, we obtain

$$\langle \psi_{\mathrm{f}}(I_{\mathrm{f}}) \rangle_\rho \quad \approx \quad \langle 1 \rangle_\rho \cdot \psi_{\mathrm{f}}(\frac{\langle I_{\mathrm{f}} \rangle_\rho}{\langle 1 \rangle_\rho}). \tag{19}$$

This approximation forms the basis of the generalized structure tensor (GST) approach, where the GST is defined as

$$\mathbf{H} = \langle \mathbf{m}_0 \otimes \mathbf{m}_0 \rangle_\rho. \tag{20}$$

The right-hand side of (19) can then be written

$$\langle 1 \rangle_\rho \cdot \psi_{\mathrm{f}}(\frac{\langle I_{\mathrm{f}} \rangle_\rho}{\langle 1 \rangle_\rho}) = \mathrm{tr}\mathbf{H} \psi_{\mathrm{f}}(\frac{\mathbf{H} : \mathbf{C}}{\mathrm{tr}\mathbf{H}}),$$

whereas the left-hand side of (19) equals $\oint_{\mathbb{U}^2} \rho \psi_{\mathrm{f}}(I_{\mathrm{f}}) d\omega$. Therefore (19) approximates the total angularly integrated fiber strain energy by strain energy computed via a GST.

In a material reinforced by fiber families with potentials $\psi_{\mathrm{f}}^{(i)}$ and ODFs $\rho^{(i)}$, we define for each fiber family a GST as $\mathbf{H}^{(i)} = \langle \mathbf{m}_0 \otimes \mathbf{m}_0 \rangle_{\rho^{(i)}}$. These GSTs are objective and symmetric tensors, do not depend on the deformation, and serve as an alternative representation of structural data (see Remark below). The total fiber energy reads

$$\Psi_{\mathrm{f}} = \sum_i \mathrm{tr}\mathbf{H}^{(i)} \cdot \psi_{\mathrm{f}}^{(i)}(\frac{\mathbf{H}^{(i)}}{\mathrm{tr}\mathbf{H}^{(i)}} : \mathbf{C}), \tag{21}$$

and the stress is given by

$$\boldsymbol{\sigma}_{\mathrm{f}} = 2\mathbf{F} \left(\sum_i \mathbf{H}^{(i)} \psi_{\mathrm{f}}^{(i)\prime}(\mathbf{H}^{(i)} : \mathbf{C}/\mathrm{tr}\mathbf{H}^{(i)}) \right) \mathbf{F}^T. \tag{22}$$

The approach that uses (20) together with (21), (22) is henceforth referred to as *the GST approach*. Note that if the ODFs $\rho^{(i)}$ satisfy (5), the term $\mathrm{tr}\mathbf{H}^{(i)} = 1$ can be omitted in (21), (22).

Although the GST approach can be thought as an independent way to model anisotropic material behavior, we prefer to regard it, based on (19), as an approximation to the AI approach. For a discussion of adequacy and accuracy of the GST model see *e.g.* [3, 7, 20, 30]. See also [30, 2] for an extended approach that takes into account higher-order terms in the expansion (17).

It has been noted by Cortes et al. [3] that the AI and GST formulations are equivalent in the case of spherical deformations and in the absence of dispersion (*i.e.* perfect fiber alignment). They also showed a clear difference between the two approaches in the case of isotropic fiber distribution, where, unlike the AI approach, the GST approach predicts that the second Piola-Kirchhoff stress is isotropic for all deformations. This illustrates well the problem of compressed fibers: for some deformations a very small portion of fibers is extended and generates stress, whereas the majority of fibers are compressed and relaxed (according to the AI). Nevertheless, the great tensile stress generated by the extended fibers is redistributed by the GST over all the fibers, as if the contracted fibers responded with a tensile stress.

From a computational point of view, the GST approach is vastly superior, as the angular integration has to be performed only once, to compute the GSTs, which stay constant for all deformations, as long as $\rho^{(i)}$ do not change. Also, the derivative of fiber potential $\psi_{\mathrm{f}}^{(i)\prime}$ needs to be evaluated only once for a given value of the deformation tensor $\mathbf{C}$. These two circumstances make it impossible to selectively exclude the response of compressed fraction of fibers. A mechanism that accounts for compressed fibers in the case of axisymmetrical ODFs has been suggested by Gasser et al. [10] and Holzapfel and Ogden [20]. We discuss it below and later consider an alternative approach.

Remark. If all the fibers are mechanically equivalent, the number of families and their split into families is somewhat arbitrary. The split does not matter in the AI model, but has an effect in the GST approach. The number of families and the distribution of fibers over them can be motivated, for example, by a desire to approximate the observed real-world structural data by transversely isotropic ODFs. Also note that the symmetric tensor $\mathbf{H}$ can be regarded as an operator, whose linear nature reduces the structural description of a fiber family from a function $\rho(\mathbf{m}_0)$ to six scalar components. The cardinality of the set of all possible $\mathbf{H}$ is less than the cardinality of the set of all admissible $\rho(\mathbf{m}_0)$, therefore the loss of information in structural data associated with the linearization (19) is unavoidable.

2.4 GST for axisymmetric dispersion and accounting for contracted fibers (GSTx)

Of particular interest are transversely isotropic, or axisymmetric, ODFs

$$\rho^{(i)}(\mathbf{m}_0) = \tilde{\rho}^{(i)}(\theta) = \tilde{\rho}^{(i)}(-\theta), \quad \theta = \arccos(\mathbf{m}_0.\mathbf{a}_0), \tag{23}$$

which define a fiber dispersion around the mean fiber directions $\mathbf{a}_0^{(i)}$. GSTs for such ODFs take the special form

$$\mathbf{H}^{(i)} = \kappa^{(i)}\mathbf{1} + (1 - 3\kappa^{(i)})\mathbf{a}_0^{(i)} \otimes \mathbf{a}_0^{(i)}, \tag{24}$$

where $\kappa^{(i)} = \pi \int_0^\pi \tilde{\rho}^{(i)}(\theta) \sin^3\theta d\theta \in [0, \frac{1}{2}]$ is the dispersion parameter [10]. The complete alignment in the direction $\mathbf{a}_0^{(i)}$, the isotropic distribution, and the complete alignment in the plane perpendicular to $\mathbf{a}_0^{(i)}$ correspond to the values $\kappa^{(i)} = 0, \frac{1}{3}, \frac{1}{2}$ respectively [20]. Apart from the case $\kappa^{(i)} = 0$ and $\frac{1}{2}$ different distributions may lead to the same parameter $\kappa^{(i)}$. For example, the value $\kappa^{(i)} = \frac{1}{3}$ also corresponds to the case when the fiber distribution forms a cone, whose generatrix and axis make an angle $\Theta^* = \arctan\sqrt{2}$, *i.e.* $\tilde{\rho}(\theta) = \delta(\Theta^* - \theta)$. This angle is known as the *magic angle* and arises in various areas, see *e.g.* [17, 12].

The form of the GST in (24) allows to express the mean square of fiber stretch through the invariants of a transversely reinforced material, $I_1 = \mathrm{tr}\mathbf{C}$, $I_4^{(i)} = \mathbf{a}_0^{(i)} \otimes \mathbf{a}_0^{(i)} : \mathbf{C}$,

$$\langle I_f \rangle_{\rho^{(i)}} = \mathbf{H}^{(i)} : \mathbf{C} = (1 - 3\kappa^{(i)})I_4^{(i)} + \kappa I_1. \tag{25}$$

It also makes possible to address the issue of compressive fiber response by annihilating the anisotropic part of $\mathbf{H}$ if the stretch in the main direction is compressive ($\mathbf{a}_0 \otimes \mathbf{a}_0 : \mathbf{C} - 1 < 0$), as suggested by Gasser et al. [10] and Holzapfel and Ogden [20], in which case we have

$$\mathbf{H}^{(i)} = \begin{cases} \kappa^{(i)}\mathbf{1} + (1 - 3\kappa^{(i)})\mathbf{a}_0^{(i)} \otimes \mathbf{a}_0^{(i)}, & \mathbf{a}_0^{(i)} \otimes \mathbf{a}_0^{(i)} : \mathbf{C} > 1, \\ \kappa^{(i)}\mathbf{1}, & \mathbf{a}_0^{(i)} \otimes \mathbf{a}_0^{(i)} : \mathbf{C} \leq 1, \end{cases} \tag{26}$$

and equations (21), (22) should be used as before.

Holzapfel and Ogden [20] observed that values of κ from $(\frac{1}{3}, \frac{1}{2}]$ yield negative pressure in an inflated thin-walled tube and concluded that these values are therefore unphysical. Similarly, in the uniaxial tension along the main fiber direction a physically meaningless combination of negative stress $\sigma < 0$ and positive strain $\lambda > 1$ can be observed for $\kappa \in (\frac{1}{3}, \frac{1}{2}]$. This can be understood by considering the following setup. Let $\mathbf{a}_0 = (1, 0, 0)$, $\mathbf{F} = \mathrm{diag}(\lambda, \lambda^{-1/2}, \lambda^{-1/2})$, $\boldsymbol{\sigma} = \mathrm{diag}(\sigma, 0, 0)$, and neglect the role of the ground substance other than the

incompressibility. From (1) and (24) we have

$$I_{\mathrm{f}} = (1-2\kappa)\lambda^2 + 2\kappa\lambda^{-1}, \tag{27}$$

$$\sigma = \left((1-2\kappa)\lambda^2 - \kappa\lambda^{-1}\right)\psi_{\mathrm{f}}'(I_{\mathrm{f}}). \tag{28}$$

It follows that

$$I_{\mathrm{f}} - 1 \leq 0 \quad \Leftrightarrow \quad \kappa \geq \frac{\lambda+\lambda^2}{2(1+\lambda+\lambda^2)}, \tag{29}$$

$$\left((1-2\kappa)\lambda^2 - \kappa\lambda^{-1}\right) \leq 0 \quad \Leftrightarrow \quad \kappa \geq \frac{\lambda^3}{2\lambda^3+1}, \tag{30}$$

which implies that σ changes sign at both $\kappa = \lambda^3/(2\lambda^3+1)$ and $\kappa = (\lambda+\lambda^2)/(1+\lambda+\lambda^2)/2$, given that $\mathrm{sgn}(\psi_{\mathrm{f}}') = \mathrm{sgn}(I_{\mathrm{f}}-1)$. The corresponding values of λ belong to the interval $(1,+\infty)$ if $\kappa > \frac{1}{3}$ and to the interval $(0,1)$ if $\kappa < \frac{1}{3}$. Thus, we have a region with negative stress and positive strain (Figure 2.a, solid line) for $\kappa > \frac{1}{3}$. For $\kappa < \frac{1}{3}$ we observe the converse situation, *i.e.* tensile stress in the contracted direction (Figure 2.b, solid line). However, when one computes the GST using (26) instead of (24), contraction in the axial direction always results in compressive stress (Figure 2.b, dashed line). The analogy between extension or contraction in the mean fiber direction and the values $\kappa > \frac{1}{3}$ or $\kappa < \frac{1}{3}$ together with respect to the exclusion of compressed fibers suggests that the issue is not in the values $\kappa \in (\frac{1}{3}, \frac{1}{2}]$ *per se*, but rather in the GST definition (26), which requires different refinement to treat appropriately compressed fibers for $\kappa \in (\frac{1}{3}, \frac{1}{2}]$. We propose to correct this problem by defining the GST for transversely isotropic fiber distribution as

$$\mathbf{H}^{(i)} = \begin{cases} \kappa^{(i)}\mathbf{1} + (1-3\kappa^{(i)})\mathbf{a}_0^{(i)} \otimes \mathbf{a}_0^{(i)}, & (1-3\kappa^{(i)})\left(\mathbf{a}_0^{(i)} \otimes \mathbf{a}_0^{(i)} : \mathbf{C} - 1\right) > 0, \\ \kappa^{(i)}\mathbf{1}, & \kappa^{(i)} \leq \frac{1}{3}, \quad \mathbf{a}_0^{(i)} \otimes \mathbf{a}_0^{(i)} : \mathbf{C} \leq 1, \\ (1-2\kappa^{(i)})\mathbf{1}, & \kappa^{(i)} > \frac{1}{3}, \quad \mathbf{a}_0^{(i)} \otimes \mathbf{a}_0^{(i)} : \mathbf{C} \geq 1. \end{cases} \tag{31}$$

This modified GST is justified by the following proposition, which considers not only transversely symmetric but rather general isochoric deformations, defined by $\det \mathbf{C} = 1$.

Proposition 1. *Let* $\mathbf{H} = \kappa\mathbf{1} + (1-3\kappa)\mathbf{a}_0 \otimes \mathbf{a}_0$. *For* $\kappa \in [0, \frac{1}{3})$

(a) all isochoric deformations that extend the main fiber direction $\mathbf{a}_0$ *(i.e.* $\mathbf{a}_0 \otimes \mathbf{a}_0 : \mathbf{C} \geq 1$*) result in an average extension of the fibers (i.e.* $\mathbf{H} : \mathbf{C} \geq 1$*);*

(b) there exist isochoric deformations that contract the main fiber direction $\mathbf{a}_0$ *(i.e.* $\mathbf{a}_0 \otimes \mathbf{a}_0 : \mathbf{C} < 1$*) and also contract the fibers on average (i.e.* $\mathbf{H} : \mathbf{C} < 1$*).*

Contrariwise, for $\kappa \in (\frac{1}{3}, \frac{1}{2}]$

(a) all isochoric deformations that contract the main fiber direction $\mathbf{a}_0$ *(i.e.* $\mathbf{a}_0 \otimes \mathbf{a}_0 : \mathbf{C} < 1$*) result in the fibers being extended on average (i.e.* $\mathbf{H} : \mathbf{C} > 1$*);*

(b) there exist isochoric deformations that extend the main fiber direction $\mathbf{a}_0$ *(i.e.* $\mathbf{a}_0 \otimes \mathbf{a}_0 : \mathbf{C} > 1$*) but contract fibers on average (i.e.* $\mathbf{H} : \mathbf{C} < 1$*).*

Proof. We demonstrate this for $\kappa < 1/3$. To ensure that the inequality

$$\mathbf{H} : \mathbf{C} - 1 = (1 - 3\kappa)(I_4 - 1) + \kappa(I_1 - 3) \geq 0 \tag{32}$$

holds, we notice that $(1 - 3\kappa)(I_4 - 1) > 0$ holds by assumption, whereas $I_1 - 3 \geq 0$ holds by virtue of incompressibility and the inequality between geometric and arithmetic means,

$$1 = \sqrt[3]{\lambda_1^2 \lambda_2^2 \lambda_3^2} \leq \frac{\lambda_1^2 + \lambda_2^2 + \lambda_3^2}{3},$$

which establishes (a).

To show (b), we construct an example. We consider a tensor $\mathbf{C}$, whose first principal axis coincides with $\mathbf{a}_0 = (1, 0, 0)$. We have $I_4 = \lambda_1^2$, $I_1 = \lambda_1^2 + \lambda_2^2 + \lambda_1^{-2}\lambda_2^{-2}$ and $\mathbf{H} : \mathbf{C} = (1 - 2\kappa)\lambda_1^2 + \kappa\lambda_2^2 + \kappa\lambda_1^{-2}\lambda_2^{-2}$. Therefore,

$$[I_{\mathrm{f}}]_{\lambda_{1,2}=1} = 1, \tag{33}$$

$$\left[\frac{d}{d(\lambda_1^2)} I_{\mathrm{f}}\right]_{\lambda_{1,2}=1} = \left[1 - 2\kappa - \kappa\lambda_1^{-4}\lambda_2^{-2}\right]_{\lambda_{1,2}=1} > 0. \tag{34}$$

Hence, there exists $\epsilon > 0$ small enough, so that $\mathbf{C} = \mathrm{diag}(1-\epsilon, 1, \frac{1}{1-\epsilon})$ implies $I_4 - 1 < 0$ and $I_{\mathrm{f}} < 1$ simultaneously. □

We conclude using the Proposition 1 that definition (31) provides a mechanism of exclusion of compressed fibers, so that an isochoric deformation always results in an average extension of fibers ($\mathbf{H}^{(i)} : \mathbf{C} \geq 1$) for any $\kappa^{(i)}$. The approach that uses (31) together with (21), (22) is later referred to as the *GSTx model*, where "x" refers to "exclusion". Similarly to the GST model, it is not necessary to integrate for each deformation, and the integration can be performed only once, to compute the dispersion parameter $\kappa^{(i)}$.

Remark. Note that the stress-strain curves shown in Figures 2.a, 2.b (dashed lines) are not smooth at $\lambda = 1$, when the anisotropic part of the GST is being excluded. Moreover, the fiber stress is, in general, discontinuous at $\mathbf{a}_0^{(i)} \otimes \mathbf{a}_0^{(i)} : \mathbf{C} = 1$, since both $I_f^{(i)} = \mathbf{H}^{(i)} : \mathbf{C}/\mathrm{tr}\mathbf{H}^{(i)}$ and $\mathbf{F}\mathbf{H}^{(i)}\mathbf{F}^T$ in (22) suffer a jump. The reason for the absence of jump in Figure 2 is that the point $\lambda = 1$ corresponded to the unstrained main fiber direction

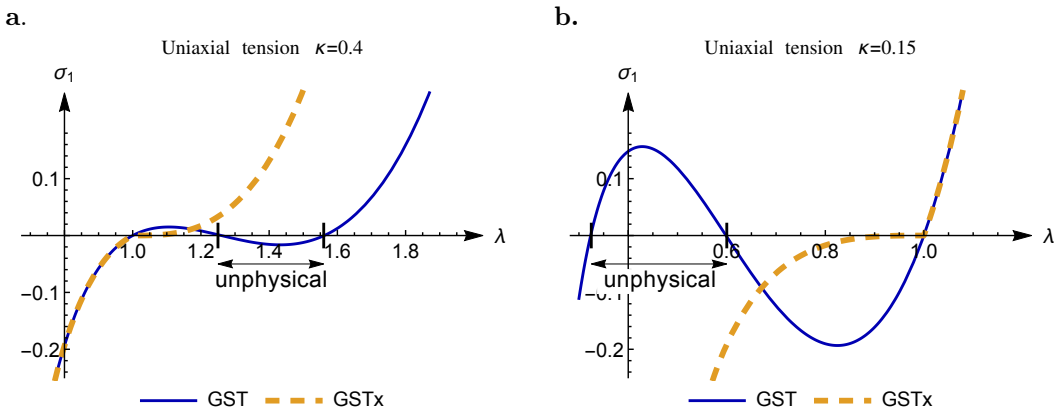

Figure 2: Material response in uniaxial tension as given by (28) with $\psi_f(I_f) = \frac{k_1}{2k_2}\exp\left[k_2(I_f-1)^2\right]$, $k_1 = 4$, $k_2 = 1$. **a**. $\kappa = .4$; **b**. $\kappa = .15$. The solid lines show the response of the model where the GST is defined by (24). The dashed lines correspond to the GST defined by (31) in **a.** and by (26) or (31) in **b**.

($\mathbf{a}_0 \otimes \mathbf{a}_0 : \mathbf{C} = 1$) and the unstrained fibers on average ($I_f = 1$) at the same time, which may not happen generally, *e.g.* when a transverse direction is subject to stretch or load. In order to remove this discontinuity, one should avoid using the second and third lines of (31) and use a different definition for the model in the region of compressed mean fiber direction. For instance, $\mathbf{F}\mathbf{H}^{(i)}\mathbf{F}^T$ and $I_f^{(i)}$ can be interpolated inside this region based on their values on the boundary of this region.

3 Alternative scheme for fiber exclusion in GST (iGST)

The compressed fibers in the GST definition (31) are taken into account after the approximation (19) was made. Alternatively, the contracted fibers can be excluded before the averaging takes place by replacing $\rho^{(i)}(\mathbf{m}_0)$ with $\chi(I_f)\rho^{(i)}(\mathbf{m}_0)$ in (15)-(19). This leads to an alternative definition of the GST:

$$\mathbf{H} = \langle \mathbf{m}_0 \otimes \mathbf{m}_0 \rangle_{\chi\rho} = \oint_{\mathbb{U}^2} \rho(\mathbf{m}_0)\chi(\mathbf{m}_0 \otimes \mathbf{m}_0 : \mathbf{C})\mathbf{m}_0 \otimes \mathbf{m}_0 d\omega. \tag{35}$$

The approach that uses (35) together with (21), (22) is referred to as *iGST* (the "i" standing for "integration").

The GST defined by (35) differs from (20) in that it implicitly depends on the deformation through the factor χ. While the GST approach averages the fiber strain over all the fibers, iGST averages it only over fibers in extension, the amount of which is given by tr$\mathbf{H}$ and depends on a particular deformation. Similarly to the AI approach, integration over the unit sphere is required for each deformation, in order to compute $\mathbf{H}$. This nullifies the main computational advantage of the GST approach. However, unlike AI, this approach requires a single evaluation of the fiber potential derivative. Therefore the iGST approach is particularly useful in detecting the effect of strong fiber dispersion, as it captures correctly fibers that are in compression, yet it is very similar to

the original GST model.

Remark. We previously mentioned that the transition from tAI to AI can be obtained using either of the substitutions (13) or (14). The iGST model is formally obtained from the GST model by (14). It suggests to investigate the outcome of applying (13) in (15)-(19). The result would be a model, identical to the GST model when the fibers are extended on average and which completely disregards fibers' presence when they are contracted on average.

4 Normal homogeneous deformations of orthotropic fiber-reinforced material

In the absence of shear the deformation gradient is given by a diagonal matrix $\mathbf{F} = \mathrm{diag}(\lambda_1, \lambda_2, \lambda_3)$, where the basis vectors $\{\mathbf{e}_1, \mathbf{e}_2, \mathbf{e}_3\}$ are defined so that they align with the principal stretch directions. For brevity, we refer to a homogeneous deformation that produces a diagonal deformation gradient simply as a diagonal deformation. Likewise, a stress state that is described by a diagonal Cauchy stress tensor in the same basis is referred to as a diagonal stress. Principal stretch directions always coincide with the principal stress directions and diagonal deformations corresponds to diagonal stresses in isotropic materials. In contrast, in an anisotropic material a diagonal deformation can give rise to non-zero shear stress components. However, a diagonal deformation always results in a diagonal stress if the material is orthotropic and the planes of symmetry are aligned with the principal stretches. In this case the Cauchy stress tensor and the left Cauchy-Green deformation tensor $\mathbf{B} = \mathbf{F}\mathbf{F}^T$ are coaxial, *i.e.* $\boldsymbol{\sigma}\mathbf{B} = \mathbf{B}\boldsymbol{\sigma}$. We note here that the the coaxiality of these tensors was analysed in details in [32] where universal relations were obtained. Our analysis could be seen as a particular case of this study.

4.1 Sufficient symmetry conditions

A material is said to be symmetric with respect to a linear transformation if the reference configuration is mapped by this transformation to another configuration which is mechanically indistinguishable from the reference configuration. The set of all such linear transformations makes up a symmetry group $\mathbb{Q} \subseteq O(3)$, and the symmetry condition reads [18]

$$W(\mathbf{F}\mathbf{Q}) = W(\mathbf{F}), \quad \forall \mathbf{Q} \in \mathbb{Q}. \tag{36}$$

The maximal possible symmetry group is $O(3)$, which corresponds to an isotropic material. As pointed earlier, ODFs satisfy $\rho(\mathbf{m}_0) = \rho(-\mathbf{m}_0)$, therefore the fiber strain energy is invariant with respect to the transformation $\mathbf{Q} = -\mathbf{1}$ (and so is the isotropic part of the strain energy). Hence, $-\mathbf{1}$ belongs to every material symmetry

group, including the minimal symmetry group, which consists of only two elements, $\mathbf{1}$ and $-\mathbf{1}$.

Next, we consider a material reinforced by m distributed families of mechanically equivalent fibers. The ith family is characterized by an ODF $\rho^{(i)}$ and a reference direction $\mathbf{a}_0^{(i)}$, which also serves as the axis of symmetry in case of a transversely isotropic distribution. For each modeling approach we formulate sufficient conditions that the ODFs must satisfy in order for the material symmetry (36) to hold. The sufficient symmetry condition for the AI approach is weaker than that for the iGST, GST and GSTx approaches (Table 2). As (36) is automatically satisfied for an isotropic material and the additive split of strain energy is assumed, condition (36) should only be applied to the anisotropic part of the strain energy.

First, consider the AI total fiber strain energy (11). We have

$$\begin{aligned}\Psi_{\mathrm{f}}(\mathbf{FQ}) &= \oint_{\mathbb{U}^2} \sum_i \rho^{(i)}(\mathbf{m}_0)\chi(\mathbf{Qm}_0 \otimes \mathbf{Qm}_0 : \mathbf{C})\psi_{\mathrm{f}}(\mathbf{Qm}_0 \otimes \mathbf{Qm}_0 : \mathbf{C})d\omega \\ &= \oint_{\mathbb{U}^2} \sum_i \rho^{(i)}(\mathbf{Qm}_0)\chi(\mathbf{m}_0 \otimes \mathbf{m}_0 : \mathbf{C})\psi_{\mathrm{f}}(\mathbf{m}_0 \otimes \mathbf{m}_0 : \mathbf{C})d\omega, \end{aligned} \tag{37}$$

where we used the identity $\mathrm{tr}\left(\mathbf{m}_0 \otimes \mathbf{m}_0 \cdot \mathbf{Q}^T\mathbf{CQ}\right) = \mathbf{Qm}_0 \otimes \mathbf{Qm}_0 : \mathbf{C}$ and then made a substitution $\mathbf{Qm}_0 \to \mathbf{m}_0$, $\mathbb{U}^2 \to \mathbf{Q}\mathbb{U}^2 = \mathbb{U}^2$. Clearly, (36) is satisfied for the AI model if the total orientation density is symmetric with respect to $\mathbf{Q}$, *i.e.*

$$\sum_{i=1}^{m} \rho^{(i)}(\mathbf{m}_0) = \sum_{i=1}^{m} \rho^{(i)}(\mathbf{Qm}_0), \quad \forall \mathbf{m}_0 \in \mathbb{U}^2, \forall \mathbf{Q} \in \mathbb{Q}. \tag{38}$$

Next, consider total fiber strain energy (21) for the iGST, GST and GSTx models,

$$\Psi_{\mathrm{f}}(\mathbf{FQ}) = \sum_i \mathrm{tr}\mathbf{H}^{(i)}(\mathbf{FQ}) \cdot \psi_{\mathrm{f}}\left(\frac{\mathbf{H}^{(i)}(\mathbf{FQ})}{\mathrm{tr}\mathbf{H}^{(i)}(\mathbf{FQ})} : \mathbf{QCQ}\right) = \sum_i \mathrm{tr}\mathbf{QH}^{(i)}(\mathbf{FQ})\mathbf{Q} \cdot \psi_{\mathrm{f}}\left(\frac{\mathbf{QH}^{(i)}(\mathbf{FQ})\mathbf{Q}}{\mathrm{tr}\mathbf{QH}^{(i)}(\mathbf{FQ})\mathbf{Q}} : \mathbf{C}\right). \tag{39}$$

The equality $\Psi_{\mathrm{f}}(\mathbf{FQ}) = \Psi_{\mathrm{f}}(\mathbf{F})$ holds if

$$\bigcup_i \mathbf{QH}^{(i)}(\mathbf{FQ})\mathbf{Q} = \bigcup_i \mathbf{H}^{(i)}(\mathbf{F}), \quad \forall \mathbf{Q} \in \mathbb{Q}. \tag{40}$$

In iGST a sufficient condition for material symmetry (36) is that the orientation density functions are globally symmetric, *i.e.*

$$\bigcup_i \rho^{(i)}(\mathbf{m}_0) = \bigcup_i \rho^{(i)}(\mathbf{Qm}_0), \quad \forall \mathbf{m}_0 \in \mathbb{U}^2, \forall \mathbf{Q} \in \mathbb{Q}, \tag{41}$$

since it implies (40), as can be seen from

$$\mathbf{Q}\mathbf{H}^{(i)}(\mathbf{F}\mathbf{Q})\mathbf{Q} = \oint_{\mathbb{U}^2} \rho^{(i)}(\mathbf{m}_0)\chi(\mathbf{Q}\mathbf{m}_0 \otimes \mathbf{Q}\mathbf{m}_0 : \mathbf{C})\mathbf{Q}\mathbf{m}_0 \otimes \mathbf{Q}\mathbf{m}_0 d\omega \tag{42}$$

$$= \oint_{\mathbb{U}^2} \rho^{(i)}(\mathbf{Q}\mathbf{m}_0)\chi(\mathbf{m}_0 \otimes \mathbf{m}_0 : \mathbf{C})\mathbf{m}_0 \otimes \mathbf{m}_0 d\omega. \tag{43}$$

By letting $\chi \equiv 1$, one arrives at the same conclusion for the GST model (20). Although the GSTx approach uses the mean fiber directions $\mathbf{a}_0^{(i)}$ in the GST definition, these directions are uniquely inferred from the transversely symmetric ODFs $\rho^{(i)}$ (with the exception of an isotropic fiber distribution case) and an additional symmetry restriction on fiber directions $\mathbf{a}_0^{(i)}$ are unnecessary. Thus, the global symmetry of orientation density functions (41) is sufficient for the material symmetry condition (36) to hold in all three GST models: GST, iGST, GSTx.

Note that the condition of global symmetry (41) does not required the ODFs to be individually symmetric, *i.e.* to satisfy

$$\rho^{(i)}(\mathbf{m}_0) = \rho^{(i)}(\mathbf{Q}\mathbf{m}_0), \quad \forall i, \forall \mathbf{m}_0 \in \mathbb{U}^2, \forall \mathbf{Q} \in \mathbb{Q}. \tag{44}$$

As the global symmetry of ODFs (41) implies the symmetry of their sum (38), the restriction we obtained for GST, iGST, GSTx models is stronger than the restriction obtained for the AI approach. This difference is a consequence of that the averaging (19) in GST approaches is done in each family individually and the result depends on how the mechanically equivalent fiber fractions are grouped into families.

4.1.1 Orthotropic material

Consider the following transformations

$$\mathbf{Q}_1 = \mathbf{1}, \qquad \mathbf{Q}_2 = \mathrm{diag}(1,-1,1), \qquad \mathbf{Q}_3 = \mathrm{diag}(1,-1,-1), \qquad \mathbf{Q}_4 = \mathrm{diag}(1,1,-1), \tag{45}$$

$$\mathbf{Q}_5 = \mathrm{diag}(-1,1,1), \qquad \mathbf{Q}_6 = \mathrm{diag}(-1,-1,1), \qquad \mathbf{Q}_7 = -\mathbf{1}, \qquad \mathbf{Q}_8 = \mathrm{diag}(-1,1,-1). \tag{46}$$

The orthotropic symmetry group $\mathbb{Q}_O = \{\mathbf{Q}_1, \ldots, \mathbf{Q}_8\}$ is generated by the reflections with respect to the coordinate planes, $\mathbf{Q}_2$, $\mathbf{Q}_4$, $\mathbf{Q}_5$, [36]. We number $\mathbf{Q}_k$, $k = 1, \ldots, 8$ in accordance with the numbering of octants (see Figure 3) and call them reflections for brevity, although the group includes proper rotations too. Some basic properties of the reflections are: *(i)* a reflection is its own inverse and transpose, *i.e.* $\mathbf{Q}_k^{-1} = \mathbf{Q}_k^T = \mathbf{Q}_k, \quad \forall k$; *(ii)* any two reflections commute, *i.e.* $\mathbf{Q}_k\mathbf{Q}_l = \mathbf{Q}_l\mathbf{Q}_k, \quad \forall k, l$; *(iii)* a reflection applied to the group bijectively maps it to itself, *i.e.* $\cup_k \mathbf{Q}_l\mathbf{Q}_k = \cup_k \mathbf{Q}_k, \quad \forall l$; *(iv)* being an orthogonal transformation, a reflection maps the unit sphere to itself, *i.e.* $\mathbf{Q}_k\mathbb{U}^2 = \mathbb{U}^2$.

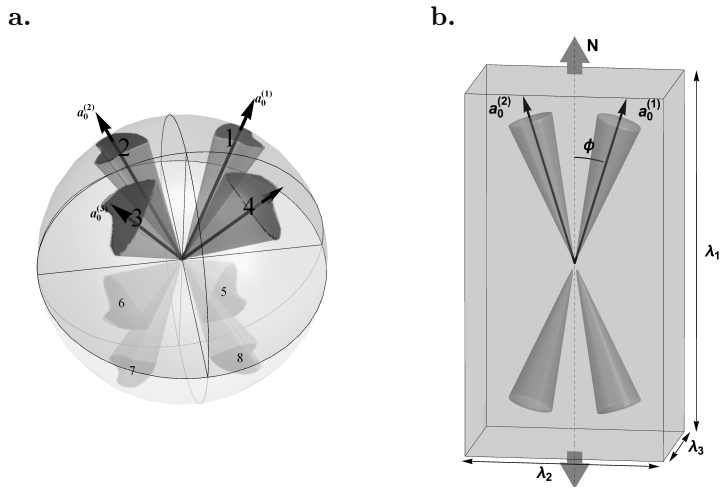

Figure 3: **a.** A schematic representation of an orthotropically symmetric fiber-reinforcement in a material with four families of fibers. Each family is characterized by its reference direction $\mathbf{a}_0^{(i)}$ and orientation density function $\rho^{(i)}(\mathbf{m}_0)$. The ODFs $\rho^{(i)}(\mathbf{m}_0)$ do not have to define transversely isotropic distributions, but must be symmetrically arranged (depicted as irregular shapes). Single digits number the octants. Fibers in the lower hemisphere (pale) are the extensions of the fibers in the upper hemisphere beyond the center of the sphere, the former can be obtained from the latter by applying transformation $\mathbf{Q}_7 = -\mathbf{1}$. The related identity $\rho^{(i)}(\mathbf{m}_0) = \rho^{(i)}(-\mathbf{m}_0)$ holds for each fiber family. **b.** A material reinforced by two families of mechanically equivalent fibers is in uniaxial tension, subject to the axial load N. Both fiber families are transversely isotropic and described by the von Mises distribution with the concentration parameter b. The mean fiber directions $\mathbf{a}_0^{(i)}$ are aligned symmetrically with respect to the principal directions, making angle ϕ with the direction of applied load. The material is orthotropic, and transverse isotropy is only observed for $\phi = 0, \pi/2$.

In order to know if condition (36) holds for each element of a group, it is only necessary to check it for the generators of the group. In the case of orthotropic symmetry ($\mathbb{Q} = \mathbb{Q}_O$), it is only necessary to check condition (36) for $\mathbf{Q}_2$, $\mathbf{Q}_4$, as $\mathbf{Q}_5 = \mathbf{Q}_2\mathbf{Q}_4\mathbf{Q}_7$ and this condition is automatically satisfied for $\mathbf{Q}_7 = -\mathbf{1}$.

A tensor $\mathbf{A}$ is diagonal in the basis $\{\mathbf{e}_1, \mathbf{e}_2, \mathbf{e}_3\}$ if and only if $\mathbf{A} = \mathbf{Q}\mathbf{A}\mathbf{Q}^T$ for all $\mathbf{Q} \in \mathbb{Q}_O$. It is not difficult to show that a diagonal deformation gradient in an orthotropic material leads to a diagonal Cauchy stress (see Proposition 2 in the Appendix). The converse is also true, therefore this relation between deformation gradients and Cauchy stress tensors can be alternatively taken as a definition of the material symmetry, from which condition (36) follows (see *e.g.* [36]). Thus a diagonal deformation results in a diagonal stress if condition (38) is satisfied when using the AI model, and condition (41) is satisfied when using iGST, GSTx, GST models.

4.1.2 An example of orthotropically symmetric fiber arrangement

Consider a material reinforced by $m = 4$ families of fibers. We pick a characteristic direction $\mathbf{a}_0^{(1)}$ for the first family of fibers. Let $\mathbf{R}_1 \in SO(3)$ be a rotation, which transforms $\mathbf{e}_1$ to $\mathbf{a}_0^{(1)}$, *i.e.* $\mathbf{a}_0^{(1)} = \mathbf{R}_1\mathbf{e}_1$. We define

rotations $\mathbf{R}_i$ and fiber directions $a_0^{(i)}$ (see Figure 3.a) by

$$\mathbf{R}_i = \mathbf{Q}_i \mathbf{R}_1 \mathbf{Q}_i, \tag{47}$$

$$\mathbf{a}_0^{(i)} = \mathbf{R}_i \mathbf{e}_1, \qquad i = 2, 3, 4. \tag{48}$$

That is,

$$\mathbf{a}_0^{(1)} = \begin{pmatrix} \cos\alpha \\ \sin\alpha\cos\beta \\ \sin\alpha\sin\beta \end{pmatrix}, \quad \mathbf{a}_0^{(2)} = \begin{pmatrix} \cos\alpha \\ -\sin\alpha\cos\beta \\ \sin\alpha\sin\beta \end{pmatrix}, \quad \mathbf{a}_0^{(3)} = \begin{pmatrix} \cos\alpha \\ -\sin\alpha\cos\beta \\ -\sin\alpha\sin\beta \end{pmatrix}, \quad \mathbf{a}_0^{(4)} = \begin{pmatrix} \cos\alpha \\ \sin\alpha\cos\beta \\ -\sin\alpha\sin\beta \end{pmatrix}. \tag{49}$$

The rotation $\mathbf{R}_i$ also relates the ODFs in families' coordinates (*i.e.* relatively to $\mathbf{a}_0^{(i)}$) and in material coordinates (*i.e.* relatively to $\mathbf{e}_1$), we have

$$\rho^{(i)}(\mathbf{m}_0) = \rho_i(\mathbf{R}_i^T \mathbf{m}_0), \qquad i = 1, \ldots, 4. \tag{50}$$

Furthermore, the ODFs in families' coordinates are also symmetric, *i.e.*

$$\rho_i(\mathbf{m}_0) = \rho(\mathbf{Q}_i \mathbf{m}_0). \tag{51}$$

As a result, conditions (41) and (38) are satisfied for this material. Indeed, we have

$$\bigcup_{i=1}^{m} \rho^{(i)}(\mathbf{Q}_k \mathbf{m}_0) = \bigcup_{i=1}^{m} \rho(\mathbf{Q}_i \mathbf{R}_i^T \mathbf{Q}_k \mathbf{m}_0) = \bigcup_{i=1}^{m} \rho(\mathbf{Q}_i \mathbf{Q}_i \mathbf{R}_1^T \mathbf{Q}_i \mathbf{Q}_k \mathbf{m}_0) = \bigcup_{p=1}^{m} \rho(\mathbf{R}_1^T \mathbf{Q}_p \mathbf{m}_0), \qquad \forall i, \tag{52}$$

and

$$\bigcup_{i=1}^{m} \rho^{(i)}(\mathbf{m}_0) = \bigcup_{i=1}^{m} \rho(\mathbf{Q}_i \mathbf{R}_i^T \mathbf{m}_0) = \bigcup_{i=1}^{m} \rho(\mathbf{Q}_i \mathbf{Q}_i \mathbf{R}_1^T \mathbf{Q}_i \mathbf{m}_0) = \bigcup_{i=1}^{m} \rho(\mathbf{R}_1^T \mathbf{Q}_i \mathbf{m}_0), \qquad \forall i. \tag{53}$$

We conclude that condition (41) holds and condition (38) follows from it. Thus, this material is orthotropically symmetric for all the dispersion models.

5 Uniaxial tension of a material with two families of fibers

5.1 Fiber reinforced material with two families of fibers

An important example of a fiber reinforced material is a material with two families of fibers. This type of material has been used to model various soft biological tissues, including human annulus fibrosus [39], cornea [1]

and arterial wall [20]. Among materials reinforced by axisymmetrically distributed fibers, this is the simplest case of an orthotropic material: a material with one family is always transversely isotropic, whereas two equivalent fiber families guarantee that a material is orthotropic and not transversely isotropic, unless the characteristic fiber directions coincide or fibers are distributed isotropically.

In order to keep the analysis as simple as possible, yet to avoid the limitations of the transverse isotropy, for the remainder of this paper we restrict our attention to an incompressible material reinforced by two mechanically equivalent families of fibers with mean directions $\mathbf{a}_0^{(1)} = (\cos\phi, \sin\phi, 0)$, $\mathbf{a}_0^{(2)} = (\cos\phi, -\sin\phi, 0)$ (see Figure 3.b). We assume that the ODFs are transversely isotropic and defined by

$$\rho^{(1)}(\mathbf{m}_0) = \rho(\mathbf{R}_1^T\mathbf{m}_0) = \tilde{\rho}\left(\arccos(\mathbf{e}_1 \cdot \mathbf{R}_1^T\mathbf{m}_0)\right), \tag{54}$$

$$\rho^{(2)}(\mathbf{m}_0) = \rho(\mathbf{R}_1\mathbf{m}_0) = \tilde{\rho}\left(\arccos(\mathbf{e}_1 \cdot \mathbf{R}_1\mathbf{m}_0)\right), \tag{55}$$

where $\mathbf{R}_1$ is the rotation matrix by angle ϕ about the axis $\mathbf{e}_3$ and $\tilde{\rho}(\theta)$ is the von Mises distribution [10]

$$\tilde{\rho}(\theta) = \frac{\sqrt{2b}}{2\pi\sqrt{\pi}} \frac{\exp\left[b(\cos 2\theta + 1)\right]}{\mathrm{erfi}(\sqrt{2b})}, \tag{56}$$

with $\mathrm{erfi}(x) = \int_0^x \exp(t^2)dt$. The degree of fiber dispersion is defined by the concentration parameter b. As noted in [19], there is a one-to-one correspondence between the concentration parameter b and the dispersion parameter κ. Note also that $\tilde{\rho}(\theta) = \tilde{\rho}(-\theta) = \tilde{\rho}(\pi + \theta)$ and that $\oint_{\mathbb{U}^2} \tilde{\rho}(\theta)d\omega = 1$.

We further assume that the matrix is *an incompressible neo-Hookean* material,

$$\psi_{\mathrm{iso}}(\mathbf{C}) = \frac{\mu}{2}(\mathrm{tr}\mathbf{C} - 1), \tag{57}$$

where μ is the shear modulus, and that the constitutive model for fibers is either the *standard reinforcing model* [37]

$$\psi_{\mathrm{std}}(I_{\mathrm{f}}) = \frac{\gamma}{2}(I_{\mathrm{f}} - 1)^2, \tag{58}$$

or the *exponential model* proposed in [19]

$$\psi_{\mathrm{exp}}(I_{\mathrm{f}}) = \frac{k_1}{2k_2}\exp[k_2(I_{\mathrm{f}} - 1)^2], \tag{59}$$

where γ, k_1 are fiber stiffness parameters of the dimension of stress and k_2 is a dimensionless parameter. As can

be seen from the derivatives of (58) and (59)

$$\frac{\partial}{\partial I_{\rm f}}\psi_{\rm std}(I_{\rm f}) = \gamma(I_{\rm f}-1), \qquad \frac{\partial}{\partial I_{\rm f}}\psi_{\rm exp}(I_{\rm f}) = k_1(I_{\rm f}-1)\exp[k_2(I_{\rm f}-1)^2], \tag{60}$$

the standard reinforcing model is a special case of the exponential model for which $k_1 = \gamma$, $k_2 = 0$.

Here we choose to study the standard reinforcing and exponential models as they have been widely studied and used in different contexts [27, 21, 20, 13, 11]. However, more recently it has been pointed out that a model that only includes the invariant I_4 is not suitable in the limit of small deformations as it does not match the expected behaviour of linear anisotropic elasticity. However, the standard reinforcing and exponential model are simple enough so that analytical progress can be achieved. We also expect that the generic features of perversions presented here will also be observed in more complicated systems as it is mainly due to a balance between nonlinearity, anisotropy and large deformations [4, 28].

Conditions (38) and (41) hold for the material, therefore the homogeneous diagonal deformations $\mathbf{F} = \mathrm{diag}(\lambda_1, \lambda_2, \lambda_3)$ correspond to a diagonal Cauchy stress $\boldsymbol{\sigma} = \mathrm{diag}(\sigma_1, \sigma_2, \sigma_3)$. The constitutive relation (8) can now be written as

$$\sigma_i(\lambda_1, \lambda_2, \lambda_3) = -p + \mu\lambda_i^2 + \sigma_{{\rm f}\,i}(\lambda_1, \lambda_2, \lambda_3), \quad i = 1, 2, 3, \tag{61}$$

where the principal stretches obey the incompressibility restriction

$$\lambda_1\lambda_2\lambda_3 = 1. \tag{62}$$

The fiber stress contribution $\sigma_{{\rm f}\,i} = 2\lambda_i^2\partial W/\partial(\lambda_i^2)$ includes the response of both families and depends on the choice of the model that accounts for fiber distribution.

For the AI model we have

$$\sigma_{{\rm f}\,i} \;=\; 4\lambda_i^2 \oint_{\mathbb{U}^2} \rho(\mathbf{m}_0)\chi(\mathbf{R}_1\mathbf{m}_0 \otimes \mathbf{R}_1\mathbf{m}_0 : \mathbf{C})\psi_{\rm f}'(\mathbf{R}_1\mathbf{m}_0 \otimes \mathbf{R}_1\mathbf{m}_0 : \mathbf{C})(\mathbf{R}_1\mathbf{m}_0)_i^2 d\omega, \tag{63}$$

where $(\mathbf{R}_1\mathbf{m}_0)_i$ denotes ith component of vector $\mathbf{R}_1\mathbf{m}_0$.

For the GST, GSTx and iGST approaches, the fiber stress reads

$$\sigma_{{\rm f}\,i} \;=\; 4\lambda_i^2 \mathrm{H}_{ii}\psi_{\rm f}'\Big(\frac{\mathbf{H} : \mathbf{C}}{\mathrm{tr}\mathbf{H}}\Big), \tag{64}$$

where $\mathbf{H} = (\mathbf{H}^{(1)} + \mathbf{H}^{(2)})/2$ is a diagonal tensor, whose exact form depends on the variant of GST approach

considered. For the GST model, we have

$$\mathrm{H}_{11} = \kappa + (1-3\kappa)\cos^2\phi, \quad \mathrm{H}_{22} = \kappa + (1-3\kappa)\sin^2\phi, \quad \mathrm{H}_{33} = \kappa. \tag{65}$$

In the GSTx approach the components of $\mathbf{H}$ are given by

$$\begin{aligned} &\mathrm{H}_{11} = \kappa + (1-3\kappa)\cos^2\phi, \quad \mathrm{H}_{22} = \kappa + (1-3\kappa)\sin^2\phi, \quad \mathrm{H}_{33} = \kappa, \quad \text{if } (1-3\kappa)\left(\lambda_1\cos^2\phi + \lambda_2\sin^2\phi - 1\right) > 0, \\ &\mathrm{H}_{11} = \kappa, \quad \mathrm{H}_{22} = \kappa, \quad \mathrm{H}_{33} = \kappa, \qquad \text{otherwise.} \end{aligned} \tag{66}$$

In the iGST approach $\mathbf{H}$ is given through the integral over the unit sphere

$$\mathrm{H}_{ii} \;=\; \oint\limits_{\mathbb{U}^2} \rho(\mathbf{m}_0)\chi(\mathbf{R}_1\mathbf{m}_0 \otimes \mathbf{R}_1\mathbf{m}_0 : \mathbf{C})(\mathbf{R}_1\mathbf{m}_0)_i^2 d\omega. \tag{67}$$

5.2 Comparison of the models in uniaxial tension

We apply a reference load $N > 0$ to the material in the direction $\mathbf{e}_1$ and leave the lateral faces traction free (Figure 3.b). That is, we have the following equations for the principal stresses

$$\sigma_1 = N\lambda_1, \quad \sigma_2 = 0, \quad \sigma_3 = 0, \tag{68}$$

where the unknowns are the Lagrangian multiplier p and any two principal stretches (*e.g.* λ_1, λ_3), while the remaining principal stretch is determined by them via (62). After eliminating the Lagrangian multiplier p from the system using $\sigma_3 = 0$, equations (68) become

$$N\lambda_1 \;=\; \sigma_1(\lambda_1, \lambda_3), \tag{69}$$

$$0 \;=\; \sigma_2(\lambda_1, \lambda_3). \tag{70}$$

5.2.1 Transversely isotropic case

As a preliminary step in the comparison of the models, we neglect the ground substance response ($\mu = 0$) and consider the transversely isotropic case $\phi = 0$, when the two fiber families are aligned and can be regarded as a single family. The symmetry implies $\lambda_2 = \lambda_3 = \lambda_1^{-1/2}$, and the deformation is completely defined by a stretch in one direction. We plot the axial Cauchy stress component as a function of the engineering strain $\varepsilon = \log\lambda_1$ for axial fiber alignment (Figure 5.a) [30]. In order to focus on the effect of fiber dispersion, we ignore the strain energy component of the ground substance, whose only contribution to the material behavior is the

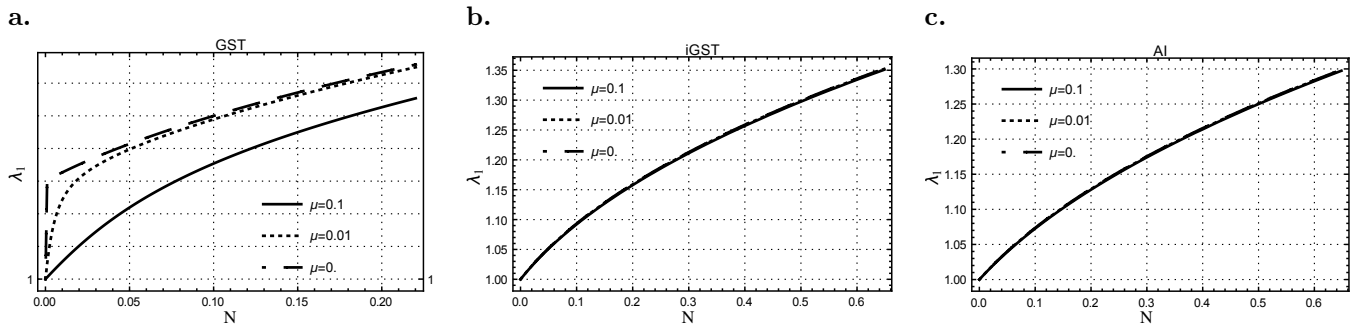

Figure 4: Response of a material (orthotropically, but not transversely symmetric) in uniaxial tension, $\phi = \pi/4$, $b = 2$, $k_2 = 0$, **(a)** GST, **(b)** iGST, **(c)** AI. If the elastic response of the ground substance is neglected, then the GST model predicts finite strain for infinitesimal load (**a**, case $\mu = 0$).

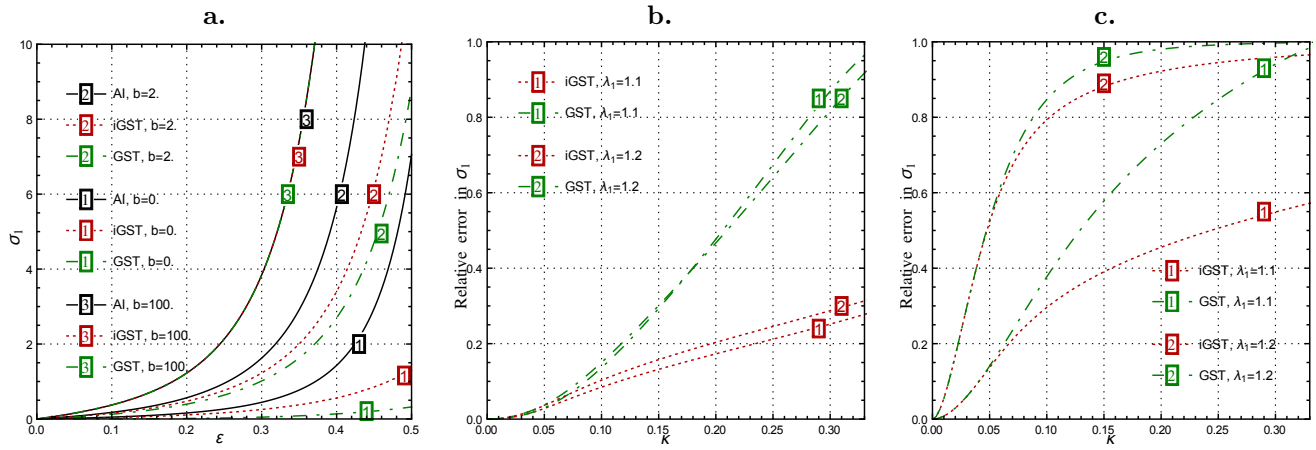

Figure 5: The comparison of different models in uniaxial tension along the mean fiber direction. (**a**) The stress in uniaxial tension versus the logarithm of the stretch. (**b**,**c**) Error in the response provided by the iGST and GST models relative to the response of the AI model as a function of fiber dispersion for constant axial stretch values $\lambda_1 = 1.1$ and $\lambda_1 = 1.2$: (**b**) soft fiber response, $k_2 = 1$; (**c**) stiff fiber response $k_2 = 30$. (Compare to Fig. 3, 4 in [30])

incompressibility. We also plot the relative error of various models with respect to AI as a function of fiber dispersion parameter (Figure 5.b, c).

Remark. If the ground substance is neglected then equation (70) for the GST model becomes $(\lambda_1^{-2}\lambda_3^{-2}\mathrm{H}_{22} - \lambda_3^2\mathrm{H}_{33})\psi_{\mathrm{f}}'(\mathbf{H} : \mathbf{C}) = 0$. It follows that the solution continuously passes through the unstrained state $\lambda_1 = \lambda_3 = 1$ only if $\mathrm{H}_{22} = \mathrm{H}_{33}$, *i.e.* the material is transversely isotropic with respect to the direction of loading. The stress-strain curves for various values of μ are shown in Figure 4. This unrealistic behavior, consisting in instantaneous large deformation for small applied loads, is only peculiar to the GST model, while the nonlinearities in the AI and iGST models allow for continuous deformation at high fiber dispersions.

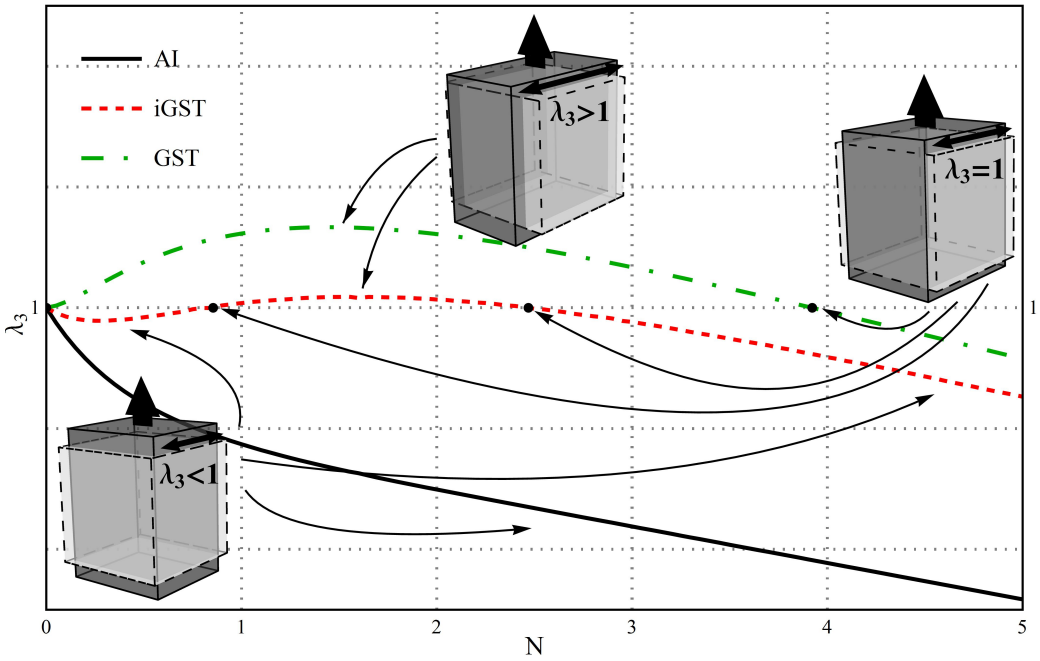

Figure 6: The dependence of the transverse stretch λ_3 on the axial load N in uniaxial tension. The perversion points are indicated with black. Different models for fiber dispersion result in qualitatively different material behavior (*i.e.* different number of perversion points), although the difference in stretch λ_3 does not exceed 6%.

5.2.2 Perversion points of the transverse strain

Extension in the transverse direction under positive axial load N is not possible in isotropic and transversely isotropic (axially symmetric) incompressible materials. That is, generically we have $\lambda_1 > 1 > \lambda_2, \lambda_3$. However, if the transverse isotropy is broken, the tensile axial load may cause the material to extend in the transverse direction $\mathbf{e}_3$, so that the principal stretches satisfy $\lambda_1, \lambda_3 > 1 > \lambda_2$. Moreover, the same material can switch between extension and contraction in this direction as the load increases. We refer to such qualitative change as a *perversion point*, which is defined in [12] as a point at which a strain passes through a distinguished value. In our case the distinguished value of stretch is $\lambda_3 = 1$, as it corresponds to the undeformed and unloaded state. As illustrated in Figure 6, the material can have multiple perversion points. The existence and number of perversion points depends on the amount of fibers, fiber stiffness, fiber dispersion and the approach chosen to model the distributed fibers. That is, different models can predict different numbers of perversion points for the same set of material parameters (Figure 6). This suggests that the number of perversion points can be used as a qualitative measure of agreement between various models, which is specific to the case when the material symmetry is weaker than transverse isotropy.

Equations (69), (70) at a perversion point ($\lambda_3 = 1$) can be written as

$$N\lambda_1 = \sigma_1(\lambda_1), \tag{71}$$

$$0 = \sigma_2(\lambda_1), \tag{72}$$

which can be solved for the axial stretch λ_1 and the load N. Note that there always exists a trivial solution $\lambda_1 = 1$, $N = 0$, which is ignored and not counted, and that equation (72) is decoupled from (71) and can be solved independently. Given that the material obeys the tension-extension inequalities, the number of perversion points when $N > 0$ equals to the number of roots of (72) that satisfy $\lambda_1 > 1$.

Since rescaling the stress will not affect the number of perversion points, we let $k_1 = \gamma = 1$ in the fiber potentials (58), (59). The role of shear modulus μ is then to control the relative amount of fibers with respect to the ground substance. The values $\mu = +\infty$ and $\mu = 0$ correspond, respectively, to an isotropic Neo-Hookean material and an incompressible material composed entirely of fiber.

We first focus on the case of the standard reinforcing model ($k_2 = 0$). The three remaining material parameters form the parametric space (ϕ, μ, b), which is divided into regions corresponding to different number of perversion points. The algebraic multiplicity of perversion points is at least two at the borders between these regions. Therefore the borders are given by

$$\sigma_2(\lambda_1) = 0, \tag{73}$$

$$\sigma_{21}(\lambda_1) = 0, \tag{74}$$

where $\sigma_{21}(\lambda_1) = \frac{d\sigma_2(\lambda_1)}{d\lambda_1}$, $\sigma_{22}(\lambda_1) = \frac{1}{2}\frac{d^2\sigma_2(\lambda_1)}{d\lambda_1^2}$ are the coefficients in the Taylor expansion

$$\sigma_2(\lambda_1 + \triangle\lambda_1) = \sigma_2(\lambda_1) + \triangle\lambda_1\sigma_{21}(\lambda_1) + \triangle\lambda_1^2\sigma_{22}(\lambda_1) + O(\triangle\lambda_1^3). \tag{75}$$

As mentioned previously, the stress in the GSTx model can have discontinuities when $\lambda_1 = \tan\phi$. If the jump occurs across the λ_1-axis then it is counted as a perversion point, therefore the condition

$$\sigma_2(\tan\phi + 0) = 0 \quad \text{or} \quad \sigma_2(\tan\phi - 0) = 0, \tag{76}$$

must be used instead of the equation (74) at $\lambda_1 = \tan\phi$.

The computations for the GST model are simple and can be done analytically. With the help of (64), (73) becomes

$$\eta^2 \mathrm{H}_{22}^2 + \eta(\frac{\mu}{4} - \mathrm{H}_{11}\mathrm{H}_{22} - \mathrm{H}_{33}\mathrm{H}_{22}) + \mathrm{H}_{11}\mathrm{H}_{33} = 0, \tag{77}$$

where $\eta = \lambda_1^{-2}$ and H_{ii} are constants given by (65). The number of perversions is exactly the number of roots $0 < \eta < 1$ of the quadratic polynomial in η in (77). One can formulate the conditions on the coefficients of the polynomial to have precisely 0, 1 or 2 suitable roots and obtain relations between parameters μ and ϕ. The analysis for GSTx requires to take into account some additional conditions, but is otherwise similar. The details are provided in the Appendix and the results are shown in Figure 7.a, d, f.

The analysis of the AI and iGST models is more complicated. As can be seen from (63) or (64) and (67), equations (71) and (72) contain integrals that cannot be solved analytically. A numerical root finding algorithm is required to solve the non-linear system (71), (72), see Appendix for the exact expressions used in this system.

The results for various models are shown for selected values of b in Figure 7. The diagrams for high degree of fiber alignment (*i.e.* low dispersion) are almost identical for all models and consist of three simply connected regions on the (μ, ϕ) plane, whose borders are parabola-like curves (Figure 7.a). High values of shear modulus μ indicate low fiber content and result in no perversion points, as expected for a nearly isotropic material. At lower values of μ the number of perversion points depends on the fiber orientation angle ϕ. The region of one perversion is situated predominantly in the half-plane $\phi < \pi/4$, whereas two perversion points can be observed for all angles. We note that some dispersion of fibers is required for the existence of two perversion points, since both axial stretch λ_1 and load N at the second perversion point tend to infinity in the limit of strict fiber alignment ($b \to +\infty$, $\kappa \to 0$).

The difference between the modeling approaches is apparent when the fiber dispersion is significant. As the dispersion increases (concentration b decreases), the regions corresponding to one and two perversion points shrink. This process occurs faster for the AI approach and slower for the GST and GSTx approaches (see Figures 7.b, c, d). The behavior of the iGST model is intermediate between AI and GST models. The range of fiber orientation angles ϕ corresponding to at least one perversion shrinks in AI and iGST models, but remains $(0, \pi/2)$ in the GST model. Also unlike the iGST and AI models, the GST model does not allow for a single perversion point when $\phi > \pi/4$. Two perversion points become impossible in AI and iGST models at high values of dispersion (Figure 7.e). At some higher degree of dispersion the material has zero perversion points for all values of shear modulus μ and fiber orientation angle ϕ. This is in contrast to the GST model (Figure 7.f), which allows the regions of one and two perversions for arbitrarily high fiber dispersion, unless the material is ideally isotropic or transversely isotropic. This difference between the models is also demonstrated in Figure 8, where the minimum and maximum values of μ that allow to have one or two perversion points are plotted as a function of the concentration parameter b.

We also considered the case of exponential fiber potential (59) for the GST model. We show in Figure 8 that in this case the number of perversion points is not limited to two and there exists a region corresponding to three perversion points.

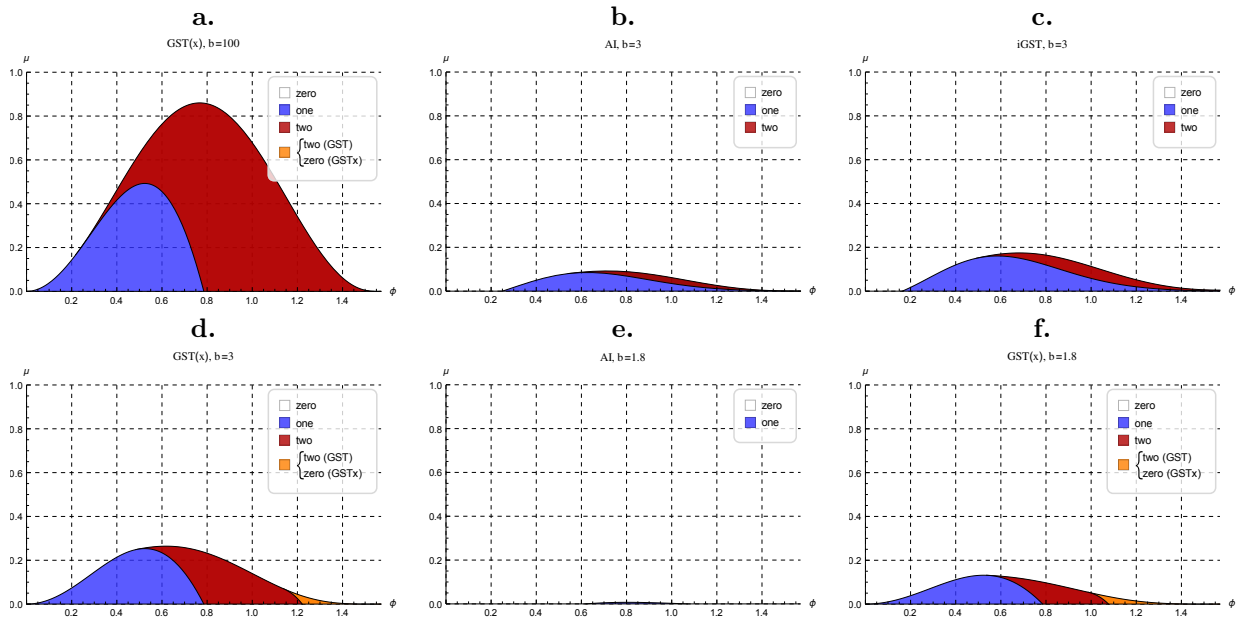

Figure 7: The number of perversion points as a function of fiber orientation angle ϕ and relative stiffness of the ground substance μ, using the standard reinforcing model ($k_2 = 0$). (**a**) Predictions of GST, iGST and AI models are very similar for high degree of fiber alignment, $b = 100$. The diagram is plotted for the GST approach. If fiber dispersion is significant, then the differences between the approaches become clear. The diagrams are shown for $b = 3$ as predicted by (**b**) AI, (**c**) iGST, (**d**) GST. For higher degrees of fiber dispersion the regions of two and one perversions shrink until they disappear from the diagram, as shown for the AI model for $b = 1.7$, (**e**). In contrast, the GST model predicts the existence of regions for $b = 1.7$ (**f**), and these regions persist for any $b > 0$.

6 Conclusion

The angular integration model (AI) allows to incorporate fiber orientation density functions into the strain energy function of a material [22]. The main disadvantage of this model is that it requires repeated numerical integrations. The generalized structure tensor model (GST) [10] lacks this disadvantage, since numerical integration is only required to compute the GST from a given fiber distribution. Thus, the GST model presents an attractive approach, which has been used to model fiber dispersion in various studies [9, 10, 29, 14, 6, 38]. However, the GST model approximates the AI model well only for low values of fiber dispersion [3]. The weighted averaging of the square of the fiber stretch over all directions as well as the inability to selectively exclude the response of compressed fiber fractions contribute to the error in the GST model. We introduce the iGST model, which disregards the contracted fiber fractions and averages the fiber stretch only over tensile directions. The models for distributed fiber we compare are summarized in Figure 1 and Table 1.

We used the problem of perversion points of the transverse strain in uniaxial tension as a qualitative measure of agreement between models for distributed fiber reinforcement, namely, the AI, GST, GSTx and iGST models. These perversion points correspond to the instants, when a progressively stretched rectangular slab expands in

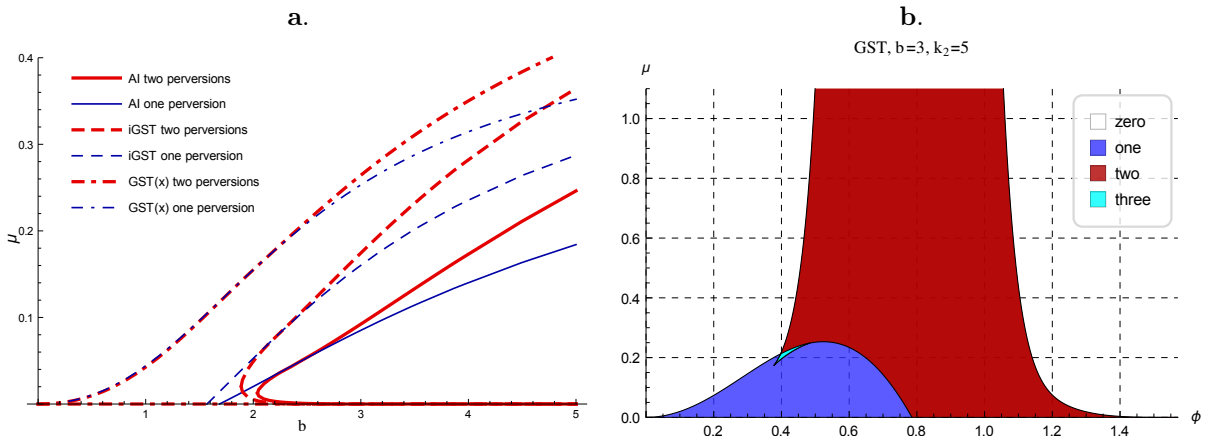

Figure 8: **a**. Extremal values of μ in the regions of one or two perversion as a function of the concentration parameter b. **b**. The number of perversion points as a function of fiber orientation angle ϕ and relative stiffness of the ground substance μ as predicted by the GST model for $b = 3$. Exponential fiber potential is used ($k_2 = 5$). In contrast to the case $k_2 = 0$, three perversion points are possible.

the direction perpendicular to the direction of applied load (Figure 6). As expected from the relative errors in stress predictions (Figure 5), the behavior of the iGST model is in between the AI and GSTx models, but is much closer to the AI model. The iGST model also possesses several distinctive features of the AI model, such as the shrinkage of the range of fiber orientation angles (Figure 7) and the existence of the maximum fiber dispersion that allows perversion points (Figure 8). The difference between the GSTx and iGST models consists in that the latter correctly addresses contracted fibers by excluding them from consideration, while the GST and GSTx models average fiber strain over both contracted and extended fibers. The largest fraction of fibers in extension is obtained when the mean fiber direction is aligned with the maximum principal stretch, hence, the accuracy of the GSTx model depends not only on the extent of dispersion, but also on the number and the arrangement of fiber families and the deformation regime. The former circumstance has been discussed *e.g.* in [7, 30], while the latter is evident from the comparison of the predictions of the GST and iGST models (Figure 7 c and f respectively) for small fiber angles ϕ and when the angle is $\phi > \frac{\pi}{4}$ or larger. Based on this argument, we advocate that the GSTx model is inaccurate comparing to the AI model when the fiber dispersion is significant primarily because it is unable to selectively disregard compressed fibers, which suggests that the GSTx model should be used only when the dispersion is low, or, at least, when most of the fibers are in extension.

Acknowledgements

AG is a Wolfson Royal Society Merit Holder and acknowledges support from a Reintegration Grant under EC Framework VII.

References

[1] V. Alastrué, B. Calvo, E. Pena, and M. Doblaré. Biomechanical modeling of refractive corneal surgery. *J. Biomech. Eng.*, 128(1):150–160, 2006.

[2] D. H. Cortes and D. M. Elliott. Accurate prediction of stress in fibers with distributed orientations using generalized high-order structure tensors. *Mech. Mater.*, 75:73–83, 2014.

[3] D. H. Cortes, S. P. Lake, J. A. Kadlowec, L. J. Soslowsky, and D. M. Elliott. Characterizing the mechanical contribution of fiber angular distribution in connective tissue: comparison of two modeling approaches. *Biomech. Model. Mechanobiol.*, 9(5):651–658, 2010.

[4] M. Destrade, B. Mac Donald, J. G. Murphy, and G. Saccomandi. At least three invariants are necessary to model the mechanical response of incompressible, transversely isotropic materials. *Comput. Mech.*, 52(4):959–969, 2013.

[5] N. J. B. Driessen, M. A. J. Cox, C. V. C. Bouten, and F. P. T. Baaijens. Remodelling of the angular collagen fiber distribution in cardiovascular tissues. *Biomech. Model. Mechanobiol.*, 7(2):93–103, 2008.

[6] S. Federico and T. C. Gasser. Nonlinear elasticity of biological tissues with statistical fibre orientation. *J. R. Soc. Interface*, 7(47):955–966, 2010.

[7] S. Federico and W. Herzog. Towards an analytical model of soft biological tissues. *J. Biomech.*, 41(16):3309–3313, 2008.

[8] P. Fratzl. *Collagen: structure and mechanics*. Springer Verlag, 2008.

[9] A. D. Freed, D. R. Einstein, and I. Vesely. Invariant formulation for dispersed transverse isotropy in aortic heart valves. *Biomech. Model. Mechanobiol.*, 4(2-3):100–117, 2005.

[10] T. C. Gasser, R. W. Ogden, and G. A. Holzapfel. Hyperelastic modelling of arterial layers with distributed collagen fibre orientations. *J. R. Soc. Interface*, 3(6):15–35, 2006.

[11] A. Goriely and M. Tabor. Spontaneous rotational inversion in phycomyces. *Phys. Rev. Lett.*, 106(13):138103, 2011.

[12] A. Goriely and M. Tabor. Rotation, inversion and perversion in anisotropic elastic cylindrical tubes and membranes. *Proc. R. Soc. A*, 469(2153):20130011, 2013.

[13] A. Goriely and R. Vandiver. On the mechanical stability of growing arteries. *IMA J. Appl. Math.*, page hxq021, 2010.

[14] R. Grytz and G. Meschke. A computational remodeling approach to predict the physiological architecture of the collagen fibril network in corneo-scleral shells. *Biomech. Model Mechanobiol.*, 9(2):225–235, 2010.

[15] Z. Y. Guo, X. Q. Peng, and B. Moran. A composites-based hyperelastic constitutive model for soft tissue with application to the human annulus fibrosus. *J. Mech. Phys. Solids*, 54(9):1952–1971, 2006.

[16] I. Hariton, G. DeBotton, T. C. Gasser, and G. A. Holzapfel. Stress-modulated collagen fiber remodeling in a human carotid bifurcation. *J. Theor. Biol.*, 248(3):460–470, 2007.

[17] J. W. Hennel and J. Klinowski. Magic-angle spinning: a historical perspective. In *New techniques in solid-state NMR*, pages 1–14. Springer, 2005.

[18] G. A. Holzapfel. *Nonlinear solid mechanics: a continuum approach for engineering.* John Wiley & Sons Ltd., 2000.

[19] G. A. Holzapfel, T. C. Gasser, and R. W. Ogden. A new constitutive framework for arterial wall mechanics and a comparative study of material models. *J. Elasticity*, 61(1-3):1–48, 2000.

[20] G. A. Holzapfel and R. W. Ogden. Constitutive modelling of arteries. *Philos. Trans. R. Soc. Lond. Ser. A Math. Phys. Eng. Sci*, 466(2118):1551–1597, 2010.

[21] C. O. Horgan and G. Saccomandi. A new constitutive theory for fiber-reinforced incompressible nonlinearly elastic solids. *J. Mech. Phys. Solids*, 53(9):1985–2015, 2005.

[22] Y. Lanir. A structural theory for the homogeneous biaxial stress-strain relationships in flat collagenous tissues. *J. Biomech.*, 12(6):423–436, 1979.

[23] Y. Lanir. Constitutive equations for fibrous connective tissues. *J. Biomech.*, 16:1–12, 1983.

[24] V. I. Lebedev and D. N. Laikov. A quadrature formula for the sphere of the 131st algebraic order of accuracy. In *Dokl. Math.*, volume 59, pages 477–481. MAIK Nauka/Interperiodica, 1999.

[25] A. V. Melnik and A. Goriely. Dynamic fiber reorientation in a fiber-reinforced hyperelastic material. *Math. Mech. Solids*, 18(6):634–648, 2013.

[26] A. Menzel. Modelling of anisotropic growth in biological tissues. A new approach and computational aspects. *Biomech. Model. Mechanobiol.*, 3(3):147–71, March 2005.

[27] J. Merodio and R. W. Ogden. Mechanical response of fiber-reinforced incompressible non-linearly elastic solids. *Int. J. Nonlin. Mech.*, 40(2):213–227, 2005.

[28] J. G. Murphy and G. Saccomandi. Exploitation of the linear theory in the non-linear modelling of soft tissue. *Math. Mech. Solids*, page 1081286514544261, 2014.

[29] A. Pandolfi and G. A. Holzapfel. Three-dimensional modeling and computational analysis of the human cornea considering distributed collagen fibril orientations. *J. Biomech. Engineering*, 130(6):061006, 2008.

[30] A. Pandolfi and M. Vasta. Fiber distributed hyperelastic modeling of biological tissues. *Mech. Mater.*, 44:151–162, 2012.

[31] R. Parrish. Lebedev quadratures on the surface of the unit sphere at double precision. `http://www.mathworks.co.uk/matlabcentral/fileexchange/27097-getlebedevsphere`, March 2010.

[32] E. Pucci and G. Saccomandi. On the use of universal relations in the modeling of transversely isotropic materials. *Int. J. Solids Struct.*, 51(2):377–380, 2014.

[33] P. Skacel and J. Bursa. Numerical implementation of constitutive model for arterial layers with distributed collagen fibre orientations. *Comput. Methods Biomech. Biomed. Engin.*, (ahead-of-print):1–13, 2013.

[34] A. J. M. Spencer. *Deformations of fibre-reinforced materials*. Oxford Univ. Press. New York, 1972.

[35] A. J. M. Spencer, editor. *Continuum theory of the mechanics of fibre-reinforced composites*, volume 282. Springer New York:, 1984.

[36] A. J. M. Spencer. *Continuum mechanics*. Courier Dover Publications, 2004.

[37] N. Triantafyllidis and R. Abeyaratne. Instabilities of a finitely deformed fiber-reinforced elastic material. *J. Appl. Mech.*, 50(1):149–156, 1983.

[38] Y. Wang, S. Son, S. M. Swartz, and N. C. Goulbourne. A mixed von mises distribution for modeling soft biological tissues with two distributed fiber properties. *Int. J. Solids Struct.*, 49(21):2914–2923, 2012.

[39] H.-C. Wu and R.-F. Yao. Mechanical behavior of the human annulus fibrosus. *J. Biomech.*, 9(1):1–7, 1976.

[40] Y. Zou and Y. Zhang. An experimental and theoretical study on the anisotropy of elastin network. *Ann. Biomed. Eng.*, 37(8):1572–1583, 2009.

Appendix

A. One useful proposition

The following proposition establishes that a diagonal deformation gradient produces a diagonal Cauchy stress tensor in an orthotropic material.

Proposition 2. *Assume (36) holds. If the deformation gradient* $\mathbf{F}$ *satisfies* $\mathbf{F} = \mathbf{Q}_k^T \mathbf{F} \mathbf{Q}_k$, $\forall \mathbf{Q}_k \in \mathbb{Q} \subset O(3)$, *then the Cauchy stress satisfies* $\boldsymbol{\sigma} = \mathbf{Q}_k^T \boldsymbol{\sigma} \mathbf{Q}_k$, $\forall \mathbf{Q}_k \in \mathbb{Q}$.

Proof. Let us denote $W_{\mathbf{F}}(\mathbf{F}) = \frac{\partial}{\partial \mathbf{F}} W(\mathbf{F})$. Then the chain rule reads $\frac{\partial}{\partial \mathbf{F}} W(\mathbf{Q}_k^T \mathbf{F} \mathbf{Q}_k) = \mathbf{Q}_k W_{\mathbf{F}}(\mathbf{F}) \mathbf{Q}_k^T$. The Cauchy stress produced by the deformation gradient $\mathbf{F}$ is

$$\boldsymbol{\sigma}(\mathbf{F}) = J^{-1} W_{\mathbf{F}}(\mathbf{F}) \mathbf{F}^T = J^{-1} \left(\frac{\partial}{\partial \mathbf{F}} W(\mathbf{F}) \right) \mathbf{F}^T, \tag{78}$$

wherein a term $-p\mathbf{1}$ must be added in the case of incompressibility. Using $\mathbf{F} = \mathbf{Q}_k^T \mathbf{F} \mathbf{Q}_k = \mathbf{Q}_k \mathbf{F} \mathbf{Q}_k^T$ and the chain rule in the above, we obtain

$$\boldsymbol{\sigma}(\mathbf{F}) = J^{-1} \left(\frac{\partial}{\partial \mathbf{F}} W(\mathbf{Q}_k^T \mathbf{F} \mathbf{Q}_k) \right) \mathbf{Q}_k \mathbf{F}^T \mathbf{Q}_k^T = J^{-1} \mathbf{Q}_k W_{\mathbf{F}}(\mathbf{F}) \mathbf{F}^T \mathbf{Q}_k^T. \tag{79}$$

Comparing (78) and (79) we conclude that

$$\boldsymbol{\sigma}(\mathbf{F}) = \mathbf{Q}_k^T \boldsymbol{\sigma}(\mathbf{F}) \mathbf{Q}_k, \quad \forall \mathbf{Q}_k \in \mathbb{Q}. \tag{80}$$

□

B. Perversion diagram for GST

The curves separating the regions of different number of perversion points in the parametric space (ϕ, μ) can be obtained analytically for the GST and GSTx models. With the notation $a = \mathrm{H}_{22}^2 > 0$, $b = \frac{\mu}{4} - \mathrm{H}_{11}\mathrm{H}_{22} - \mathrm{H}_{33}\mathrm{H}_{22}$, $c = \mathrm{H}_{11}\mathrm{H}_{33} > 0$ the left-hand side of (77) becomes

$$a\eta^2 + b\eta + c = 0, \tag{81}$$

where the roots η of this polynomial correspond to perversion points if and only if they satisfy $\eta \in (0, 1)$. The condition for existence of positive distinct roots $\eta_\pm = (-b \pm \sqrt{\Delta})/2a$ is

$$\begin{cases} \Delta = b^2 - 4ac > 0, \\ -b > 0, \end{cases} \tag{82}$$

which is equivalent to

$$\mu \leq 4\mathrm{H}_{22}(\sqrt{\mathrm{H}_{33}} - \sqrt{\mathrm{H}_{11}})^2, \tag{83}$$

where the equality corresponds to coinciding positive roots if $\mathrm{H}_{22}, \mathrm{H}_{33} \neq 0$. The requirement $\eta_+ < 1$ is equivalent to

$$\begin{cases} \mu > 4(\mathrm{H}_{22} - 2\mathrm{H}_{22}^2 - \mathrm{H}_{11}\mathrm{H}_{33}), \\ \mu > 4(\mathrm{H}_{22} - 3\mathrm{H}_{22}^2), \end{cases} \tag{84}$$

whereas the requirement $\eta_- < 1$ is equivalent to

$$\begin{bmatrix} \mu < 4(\mathrm{H}_{22} - 2\mathrm{H}_{22}^2 - \mathrm{H}_{11}\mathrm{H}_{33}), \\ \mu > 4(\mathrm{H}_{22} - 3\mathrm{H}_{22}^2). \end{bmatrix} \tag{85}$$

Here curly braces and square brackets denote logical "and" and "or" respectively. Combining the conditions, we discover that there exist two perversion points if

$$\begin{cases} \mu < 4\mathrm{H}_{22}(\sqrt{\mathrm{H}_{33}} - \sqrt{\mathrm{H}_{11}})^2, \\ \mu > 4(\mathrm{H}_{22} - 2\mathrm{H}_{22}^2 - \mathrm{H}_{11}\mathrm{H}_{33}), \\ \mu > 4(\mathrm{H}_{22} - 3\mathrm{H}_{22}^2), \end{cases} \tag{86}$$

and only one perversion if

$$\mu < 4(\mathrm{H}_{22} - 2\mathrm{H}_{22}^2 - \mathrm{H}_{11}\mathrm{H}_{33}). \tag{87}$$

Equation (81) in the case of perfect fiber alignment ($\kappa = 0$) clearly has a root $\eta = 0$, as $c = \mathrm{H}_{11}\mathrm{H}_{33} = \mathrm{H}_{11}\kappa = 0$. That is, one perversion point is achieved at the infinite axial stretch.

C. Perversion diagram for GSTx

The material in GSTx model "switches" to the isotropic behavior when $\lambda < \tan\phi$, where the notation $\lambda = \lambda_1$ is introduced. For $\lambda < \tan\phi$ we always have $\sigma_2(\lambda) < 0$, and condition (76) can only be realized through its first part. The results obtained for the GST model remain unaffected if there are zero or one perversion points or if both perversion points occur in the anisotropic regime, *i.e.* they satisfy $\lambda > \tan\phi$. If there are two perversion points according to the GST model, and only one of them lies in the region $\lambda < \tan\phi$, then the total number of perversions does not change either due to the jump from $\sigma_2(\tan\phi - 0) < 0$ to $\sigma_2(\tan\phi + 0) > 0$. In order to identify the difference between the GST and GSTx models, it only remains to consider the case when both perversion points exist and are in the region $\lambda < \tan\phi$. The corresponding condition $\eta_+ > \eta_- > \tan^{-2}\phi$ is equivalent to

$$\begin{cases} \mu < 4\left(\mathrm{H}_{22} - \mathrm{H}_{22}^2(1 + 2\tan^{-2}\phi)\right), \\ \mu > 4\mathrm{H}_{33}(\mathrm{H}_{22}\tan^{-2}\phi - \mathrm{H}_{33})(\tan^2\phi - 1). \end{cases} \tag{88}$$

This defines the region in the parameter space where the GST model predicts two perversion points, whilst the GSTx model predicts none.

D. Perversion diagram for AI, iGST

For the AI and iGST approaches one has to solve equations (73), (74) numerically. Knowing that the ground substance response is neo-Hookean, we can write (73), (74) as

$$\mu = \lambda^4 \sigma_{21\mathrm{f}}, \tag{89}$$

$$0 = \lambda^4(\lambda^{-2}-1)\sigma_{21\mathrm{f}} + \sigma_{2\mathrm{f}}, \tag{90}$$

which are decoupled and can be solved one-by-one for λ and μ, if ϕ is known. At the intersection of the curves given by (89), (90) the perversions have algebraic multiplicity of at least three and are given by

$$\sigma_2 = 0, \quad \sigma_{21} = 0, \quad \sigma_{22} = 0, \tag{91}$$

which can also be written as

$$\mu = \lambda^4 \sigma_{21\mathrm{f}}, \tag{92}$$

$$0 = \sigma_{21\mathrm{f}}\lambda^4(\lambda^{-2}-1) + \sigma_{2\mathrm{f}}, \tag{93}$$

$$0 = \sigma_{21\mathrm{f}}\lambda^{-2} + \sigma_{22\mathrm{f}}, \tag{94}$$

where the first equation is decoupled from the remaining, and the remaining two can be solved by a root finding algorithm for λ, ϕ.

One can also be interested in finding local extrema of the curves $\mu = \mu(\phi)$, which are given by $d\mu/d\phi = 0$. In order to find a convenient way to describe these extrema, we differentiate (73) and (74) to obtain

$$\frac{d}{d\phi}\sigma_2 = \frac{\partial}{\partial\phi}\sigma_2 + \frac{\partial\sigma_2}{\partial(\lambda^2)}\cdot\frac{d\lambda^2}{d\phi} + \frac{\partial\sigma_2}{\partial\mu}\cdot\frac{d\mu}{d\phi} = \sigma_{20\phi} + \sigma_{21}\cdot\frac{d\lambda^2}{d\phi}, \tag{95}$$

$$\frac{d}{d\phi}\sigma_{21} = \frac{\partial}{\partial\phi}\sigma_{21} + \frac{\partial\sigma_{21}}{\partial(\lambda^2)}\cdot\frac{d\lambda^2}{d\phi} + \frac{\partial\sigma_{21}}{\partial\mu}\cdot\frac{d\mu}{d\phi} = \sigma_{21\phi} + 2\sigma_{22}\cdot\frac{d\lambda^2}{d\phi}, \tag{96}$$

where $\sigma_{2\phi} = \partial\sigma_2/\partial\phi$, $\sigma_{21\phi} = \partial\sigma_{21}/\partial\phi$. After eliminating $d\lambda^2/d\phi$ we have $2\sigma_{22}\sigma_{20\phi} = \sigma_{21}\sigma_{21\phi}$, so that the

extrema of $\mu(\phi)$ are determined by

$$\begin{aligned} \mu &= \lambda^4 \sigma_{21\mathrm{f}}, && (97)\\ 0 &= \sigma_{21\mathrm{f}}\lambda^4(\lambda^{-2}-1)+\sigma_{2\mathrm{f}}, && (98)\\ 0 &= 2\sigma_{22}\sigma_{20\phi}-\sigma_{21}\sigma_{21\phi}. && (99) \end{aligned}$$

As before, the second and the third equations are to be solved by a root finding algorithm for λ, ϕ, after which μ is found from the first equation.

E. Expressions for the AI model

In order to express an integral over the unit sphere as an iterated integral, we introduce spherical coordinates $(\tilde{\theta},\tilde{\varphi})$ and let

$$\mathbf{m}_0 = (m_{01}, m_{02}, m_{03}) = (\sin\tilde{\theta}\cos\tilde{\varphi}, \sin\tilde{\theta}\sin\tilde{\varphi}, \cos\tilde{\theta}). \tag{100}$$

By (63), (54) we have

$$\sigma_{2\mathrm{f}} = 8\int_0^{\pi}\int_{-\tilde{\varphi}^*}^{\tilde{\varphi}^*} \rho\cdot\psi_f'\cdot(m_{02}^2\lambda^{-2}-m_{03}^2)\sin\tilde{\theta}\,d\tilde{\theta}\,d\tilde{\varphi}, \tag{101}$$

where $\tan\tilde{\varphi}^*=\lambda$, $\rho=\rho(\mathbf{R}_1^T\mathbf{m}_0)=\tilde{\rho}(\theta)$, $\theta(\tilde{\theta},\tilde{\varphi},\phi)=\arccos(\sin\tilde{\theta}\cos(\phi+\tilde{\varphi}))$, $\psi_f'=\psi_f'(\mathbf{m}_0\otimes\mathbf{m}_0:\mathbf{C})$. We also have

$$\sigma_{21\mathrm{f}} = 8\int_0^{\pi}\int_{-\tilde{\varphi}^*}^{\tilde{\varphi}^*} \rho\cdot\left[\psi_f''\cdot(m_{01}^2-m_{02}^2\lambda^{-4})(m_{02}^2\lambda^{-2}-m_{03}^2)+\psi_f'\cdot(-m_{02}^2\lambda^{-4})\right]\sin\tilde{\theta}\,d\tilde{\theta}\,d\tilde{\varphi}, \tag{102}$$

$$\begin{aligned} \sigma_{22\mathrm{f}} &= 4\int_0^{\pi}\int_{-\tilde{\varphi}^*}^{\tilde{\varphi}^*} \rho\cdot\big[\psi_f'''\cdot(m_{01}^2-m_{02}\lambda^{-4})^2(m_{02}^2\lambda^{-2}-m_{03}^2)\\ &\quad +\psi_f''\cdot 2m_{02}^2\lambda^{-4}(2m_{02}^2\lambda^{-4}-m_{01}^2-m_{03}^2\lambda^{-2})+\psi_f'\cdot 2m_{02}^2\lambda^{-6}\big]\sin\tilde{\theta}\,d\tilde{\theta}\,d\tilde{\varphi}\\ &\quad +4\int_0^{\pi}\left[\rho_{|\tilde{\varphi}=\tilde{\varphi}^*}+\rho_{|\tilde{\varphi}=-\tilde{\varphi}^*}\right]\cdot\left[\psi_f''\cdot(m_{01}^2-m_{02}^2\lambda^{-4})(m_{02}^2\lambda^{-2}-m_{03}^2)\right]_{|\tilde{\varphi}=\tilde{\varphi}^*}\frac{\sin\tilde{\theta}}{2\lambda(1+\lambda^2)}d\tilde{\theta}, \end{aligned} \tag{103}$$

$$\sigma_{2\phi} = 8\int_0^{\pi}\int_{-\tilde{\varphi}^*}^{\tilde{\varphi}^*} \rho\cdot\psi_f'\cdot(m_{02}^2\lambda^{-2}-m_{03}^2)(-2b\sin 2(\phi+\tilde{\varphi}))\sin^3\tilde{\theta}\,d\tilde{\theta}\,d\tilde{\varphi}, \tag{104}$$

$$\sigma_{21\phi} = \frac{d}{d\phi}\sigma_{21} = 8\int_0^{\pi}\int_{-\tilde{\varphi}^*}^{\tilde{\varphi}^*} \rho\cdot\left[\psi_f''\cdot(m_{01}^2-m_{02}^2\lambda^{-4})(m_{02}^2\lambda^{-2}-m_{03}^2)+\psi_f'\cdot(-m_{02}^2\lambda^{-4})\right](-2b\sin 2(\phi+\tilde{\varphi}))\sin^3\tilde{\theta}\,d\tilde{\theta}\,d\tilde{\varphi}, \tag{105}$$

$$
\begin{aligned}
\sigma_{22\phi} &= 4\int_0^{\pi}\int_{-\tilde{\varphi}^*}^{\tilde{\varphi}^*} \rho\cdot\left[\psi_f'''\cdot(m_{01}^2-m_{02}\lambda^{-4})^2(m_{02}^2\lambda^{-2}-m_{03}^2)\right.\\
&\left.+\psi_f''\cdot 2m_{02}^2\lambda^{-4}(2m_{02}^2\lambda^{-4}-m_{01}^2-m_{03}^2\lambda^{-2})+\psi_f'\cdot 2m_{02}^2\lambda^{-6}\right](-2b\sin 2(\phi+\tilde{\varphi}))\sin^3\tilde{\theta}d\tilde{\theta}\,d\tilde{\varphi} \qquad (106)\\
&+4\int_0^{\pi}[\rho_{|\tilde{\varphi}=\tilde{\varphi}^*}\sin 2(\phi+\tilde{\varphi}^*)+\rho_{|\tilde{\varphi}=-\tilde{\varphi}^*}\sin 2(\phi-\tilde{\varphi}^*)]\cdot\left[\psi_f''\cdot(m_{01}^2-m_{02}^2\lambda^{-4})(m_{02}^2\lambda^{-2}-m_{03}^2)\right]_{|\tilde{\varphi}=\tilde{\varphi}^*}\frac{-2b\sin^3\tilde{\theta}}{2\lambda(1+\lambda^2)}d\tilde{\theta},
\end{aligned}
$$

where we used

$$
\frac{d\rho}{d\phi}=\frac{d\rho}{d\tilde{\varphi}}=-2b\sin^2\tilde{\theta}\sin 2(\phi+\tilde{\varphi})\cdot\rho. \qquad (107)
$$

F. Expressions for the iGST model

Let us denote $g=\mathrm{H}_{22}\lambda^{-2}-\mathrm{H}_{33}$, $I_f=\left(\mathrm{H}_{11}\lambda^2+\mathrm{H}_{22}\lambda^{-2}+\mathrm{H}_{33}\right)/\left(\mathrm{H}_{11}+\mathrm{H}_{22}+\mathrm{H}_{33}\right)$. From (64) we have

$$
\sigma_{2\mathrm{f}}=4g\cdot\psi_f', \qquad (108)
$$

$$
\sigma_{21\mathrm{f}}=4g'\cdot\psi_f'+4g\cdot\psi_f''\cdot I_f', \qquad (109)
$$

$$
\sigma_{22\mathrm{f}}=2g''\cdot\psi_f'+2\psi_f''\left(2g'\cdot I_f'+g\cdot I_f''\right)+2g\cdot\psi_f'''\cdot I_f'^2, \qquad (110)
$$

$$
\sigma_{2\phi}=4g_\phi\cdot\psi_f'+4g\cdot\psi_f''\cdot I_{f\phi}, \qquad (111)
$$

$$
\sigma_{21\phi}=4g_\phi'\cdot\psi_f'+4\psi_f''\left(g'\cdot I_{f\phi}+g_\phi\cdot I_f'\right)+4g\cdot\psi_f'''\cdot I_f\cdot I_{f\phi}, \qquad (112)
$$

$$
\begin{aligned}
\sigma_{22\phi} &= 2g_\phi''\cdot\psi_f'+2\psi_f''\left(2g_\phi'\cdot I_f'+2g'\cdot I_{f\phi}'+g''I_{f\phi}+g_\phi\cdot I_f''+g\cdot I_{f\phi}''\right)\\
&+2\psi_f'''\cdot\left(g_\phi I_f'^2+2gI_f'I_{f\phi}'\right)+2g\psi_f''''\cdot I_f'^2 I_{f\phi}, \qquad (113)
\end{aligned}
$$

where the expressions for the derivatives of g and I_f can be computed by the chain rule. From (67) we have

$$
\begin{pmatrix}\mathrm{H}_{11}\\ \mathrm{H}_{22}\\ \mathrm{H}_{33}\end{pmatrix}=\int_0^{\pi}\int_0^{2\pi}\rho(\mathbf{m}_0)\begin{pmatrix}m_{01}^2\\ m_{02}^2\\ m_{03}^2\end{pmatrix}\sin\tilde{\theta}d\tilde{\varphi}d\tilde{\theta}=2\int_0^{\pi}\int_{-\tilde{\varphi}^*}^{\tilde{\varphi}^*}\rho\cdot\begin{pmatrix}\sin^3\tilde{\theta}\cos^2\tilde{\varphi}\\ \sin^3\tilde{\theta}\sin^2\tilde{\varphi}\\ \sin\tilde{\theta}\cos^2\tilde{\theta}\end{pmatrix}d\tilde{\varphi}d\tilde{\theta}. \qquad (114)
$$

We denote $\rho_+=\tilde{\rho}(\theta_+)$, $\theta_+=\arccos(\sin\tilde{\theta}\cos(\phi+\tilde{\varphi}^*))$,$\rho_-=\tilde{\rho}(\theta_-)$, $\theta_-=\arccos(\sin\tilde{\theta}\cos(\phi-\tilde{\varphi}^*))$, and the

derivatives of H_i are given by

$$\mathrm{H}'_{11} = \frac{1}{\lambda(1+\lambda^2)} \int_0^\pi (\rho_+ + \rho_-) \sin^3\tilde{\theta} \cos^2\tilde{\varphi}^* d\tilde{\theta} = \frac{1}{\lambda(1+\lambda^2)^2} \int_0^\pi (\rho_+ + \rho_-) \sin^3\tilde{\theta} d\tilde{\theta}, \tag{115}$$

$$\mathrm{H}'_{22} = \frac{1}{\lambda(1+\lambda^2)} \int_0^\pi (\rho_+ + \rho_-) \sin^3\tilde{\theta} \sin^2\tilde{\varphi}^* d\tilde{\theta} = \frac{\lambda}{(1+\lambda^2)^2} \int_0^\pi (\rho_+ + \rho_-) \sin^3\tilde{\theta} d\tilde{\theta}, \tag{116}$$

$$\mathrm{H}'_{33} = \frac{1}{\lambda(1+\lambda^2)} \int_0^\pi (\rho_+ + \rho_-) \sin\tilde{\theta} \cos^2\tilde{\theta} d\tilde{\theta} = \frac{\lambda}{(1+\lambda^2)} \int_0^\pi (\rho_+ + \rho_-) \sin\tilde{\theta} \cos^2\tilde{\theta} d\tilde{\theta}, \tag{117}$$

$$\mathrm{H}''_{11} = \int_0^\pi \frac{\sin^3\tilde{\theta}}{2\lambda^3(1+\lambda^2)^3} \left(\rho_+ \cdot \left[-1-5\lambda^2-2\lambda b \sin^2\tilde{\theta} \sin 2(\tilde{\varphi}^*+\phi)\right] + \rho_- \left[-1-5\lambda^2+2\lambda b \sin^2\tilde{\theta} \sin 2(-\tilde{\varphi}^*+\phi)\right]\right) d\tilde{\theta}, \tag{118}$$

$$\mathrm{H}''_{22} = \int_0^\pi \frac{\sin^3\tilde{\theta}}{2\lambda(1+\lambda^2)^3} \left(\rho_+ \cdot \left[-3\lambda^2-2\lambda b \sin^2\tilde{\theta} \sin 2(\tilde{\varphi}^*+\phi)\right] + \rho_- \left[-3\lambda^2+2\lambda b \sin^2\tilde{\theta} \sin 2(-\tilde{\varphi}^*+\phi)\right]\right) d\tilde{\theta}, \tag{119}$$

$$\mathrm{H}''_{33} = \int_0^\pi \frac{\sin\tilde{\theta}\cos^2\tilde{\theta}}{2\lambda^3(1+\lambda^2)^3} \left(\rho_+ \cdot \left[-1-3\lambda^2-2\lambda b \sin^2\tilde{\theta} \sin 2(\tilde{\varphi}^*+\phi)\right] + \rho_- \left[-1-3\lambda^2+2\lambda b \sin^2\tilde{\theta} \sin 2(-\tilde{\varphi}^*+\phi)\right]\right) d\tilde{\theta}, \tag{120}$$

$$\begin{pmatrix} \mathrm{H}_{11\phi} \\ \mathrm{H}_{22\phi} \\ \mathrm{H}_{33\phi} \end{pmatrix} = 2 \int_0^\pi \int_{-\tilde{\varphi}^*}^{\tilde{\varphi}^*} -2b \sin 2(\tilde{\varphi}+\phi)\rho \cdot \begin{pmatrix} \sin^5\tilde{\theta}\cos^2\tilde{\varphi} \\ \sin^5\tilde{\theta}\sin^2\tilde{\varphi} \\ \sin^3\tilde{\theta}\cos^2\tilde{\theta} \end{pmatrix} d\tilde{\varphi} d\tilde{\theta} \tag{121}$$

$$\mathrm{H}'_{11\phi} = \frac{-2b\sin^5\tilde{\theta}}{\lambda(1+\lambda^2)^2} \int_0^\pi \left(\rho_+ \cdot \sin 2(\tilde{\varphi}^*+\phi) + \rho_- \cdot \sin 2(-\tilde{\varphi}^*+\phi)\right) d\tilde{\theta}, \tag{122}$$

$$\mathrm{H}'_{22\phi} = \frac{-2\lambda b\sin^5\tilde{\theta}}{(1+\lambda^2)^2} \int_0^\pi \left(\rho_+ \cdot \sin 2(\tilde{\varphi}^*+\phi) + \rho_- \cdot \sin 2(-\tilde{\varphi}^*+\phi)\right) d\tilde{\theta}, \tag{123}$$

$$\mathrm{H}'_{33\phi} = \frac{-2b\lambda\sin^3\tilde{\theta}\cos^2\tilde{\theta}}{(1+\lambda^2)} \int_0^\pi \left(\rho_+ \cdot \sin 2(\tilde{\varphi}^*+\phi) + \rho_- \cdot \sin 2(-\tilde{\varphi}^*+\phi)\right) d\tilde{\theta}, \tag{124}$$

$$\mathrm{H}''_{11\phi} = \int_0^{\pi} \frac{\sin^5\tilde{\theta}}{2\lambda^3(1+\lambda^2)^3}\Big(\rho_+\cdot\Big[(-2b\sin 2(\tilde{\varphi}^*+\phi))\Big(-1-5\lambda^2-2\lambda b\sin^2\tilde{\theta}\sin 2(\tilde{\varphi}^*+\phi)\Big)-4\lambda b\cos 2(\tilde{\varphi}^*+\phi)\Big]$$
$$+\rho_-\Big[(-2b\sin 2(-\tilde{\varphi}^*+\phi))\Big(-1-5\lambda^2+2\lambda b\sin^2\tilde{\theta}\sin 2(-\tilde{\varphi}^*+\phi)\Big)+4\lambda b\cos 2(-\tilde{\varphi}^*+\phi)\Big]\Big)\,d\tilde{\theta}, \quad (125)$$

$$\mathrm{H}''_{22\phi} = \int_0^{\pi} \frac{\sin^5\tilde{\theta}}{2\lambda(1+\lambda^2)^3}\Big(\rho_+\cdot\Big[(-2b\sin 2(\tilde{\varphi}^*+\phi))\Big(-3\lambda^2-2\lambda b\sin^2\tilde{\theta}\sin 2(\tilde{\varphi}^*+\phi)\Big)-4\lambda b\cos 2(\tilde{\varphi}^*+\phi)\Big]+$$
$$+\rho_-\Big[(-2b\sin 2(-\tilde{\varphi}^*+\phi))\Big(-3\lambda^2+2\lambda b\sin^2\tilde{\theta}\sin 2(-\tilde{\varphi}^*+\phi)\Big)+4\lambda b\cos 2(-\tilde{\varphi}^*+\phi)\Big]\Big)\,d\tilde{\theta}, \quad (126)$$

$$\mathrm{H}''_{33\phi} = \int_0^{\pi} \frac{\sin^3\tilde{\theta}\cos^2\tilde{\theta}}{2\lambda^3(1+\lambda^2)^3}\Big(\rho_+\cdot\Big[(-2b\sin 2(\tilde{\varphi}^*+\phi))\Big(-1-3\lambda^2-2\lambda b\sin^2\tilde{\theta}\sin 2(\tilde{\varphi}^*+\phi)\Big)-4\lambda b\cos 2(\tilde{\varphi}^*+\phi)\Big]$$
$$+\rho_-\Big[(-2b\sin 2(-\tilde{\varphi}^*+\phi))\Big(-1-3\lambda^2+2\lambda b\sin^2\tilde{\theta}\sin 2(-\tilde{\varphi}^*+\phi)\Big)+4\lambda b\cos 2(-\tilde{\varphi}^*+\phi)\Big]\Big)\,d\tilde{\theta}. \quad (127)$$

G. A remark on computational aspects

With regard to numerics, we observe that an adaptive scheme for accurate numerical integration is required when investigating the number of perversions. Fixed grids can result in oscillations of the computed numerical value of $\sigma_2(\lambda_1)$ around the true value. These oscillations occur when a node of the grid enters the tensile region (as λ_1 increases) and the finite portion of fibers associated with the node is taken into consideration. This leads to the overestimation of the amount of tensile fibers, which is later followed by the underestimation, and then the cycle repeats with another node as the deformation proceeds. The fluctuations of numerical values of σ_2 can have a sufficiently large magnitude to cause multiple false perversion points to appear. These artifacts are associated with high fiber dispersion and are especially noticeable in the iGST approach, where (unlike the AI model) the integrand is discontinuous at the boundary of the tensile region on the unit sphere. For instance, when we use the Lebedev quadrature scheme of the 131st order of accuracy [31, 24] with 5810 nodes, the described artifacts take place for a reasonable choice of step $\triangle\lambda_1$. Skacel and Bursa [33] compared various schemes of numerical integration on the unit sphere and concluded that Lebedev quadrature achieved the best results, surpassing adaptive quadratures, yet the latter are required for the analysis of perversion points.